HHS Public Access
Author manuscript
Neuron. Author manuscript; available in PMC 2023 February 02.

Published in final edited form as:
Neuron. 2022 February 02; 110(3): 436–451.e11. doi:10.1016/j.neuron.2021.10.032.

Rescue of α-synuclein aggregation in Parkinson's patient neurons by synergistic enhancement of ER proteostasis and protein trafficking

Iva Stojkovska[1], **Willayat Y. Wani**[1], **Friederike Zunke**[1,2], **Nandkishore R. Belur**[1], **Egor A. Pavlenko**[1], **Nkatha Mwenda**[1], **Karan Sharma**[1], **Laetitia Francelle**[1], **Joseph R. Mazzulli**[1,*]

[1]The Ken and Ruth Davee Department of Neurology, Northwestern University Feinberg School of Medicine, Chicago, IL 60611, USA

[2]Department of Molecular Neurology, University Hospital Erlangen, Friedrich-Alexander University Erlangen-Nürnberg, Erlangen, Germany

Summary

Neurodegenerative disorders are characterized by a collapse in proteostasis, shown by the accumulation of insoluble protein aggregates in the brain. Proteostasis involves a balance of protein synthesis, folding, trafficking, and degradation, but how aggregates perturb these pathways is unknown. Using Parkinson's disease (PD) patient midbrain cultures, we find that aggregated α-synuclein induces endoplasmic reticulum (ER) fragmentation and compromises ER protein folding capacity, leading to misfolding and aggregation of immature lysosomal β-glucocerebrosidase. Despite this, PD neurons fail to initiate the unfolded protein response, indicating perturbations in sensing or transducing protein misfolding signals in the ER. Small molecule enhancement of ER proteostasis machinery promotes β-glucocerebrosidase solubility, while simultaneous enhancement of trafficking improves ER morphology, lysosomal function, and reduces α-synuclein. Our studies suggest that aggregated a-synuclein perturbs the ability of neurons to respond to misfolded proteins in the ER, and that synergistic enhancement of multiple proteostasis branches may provide therapeutic benefit in PD.

Graphical Abstract

*Lead Contact: Joseph R. Mazzulli, PhD, The Ken and Ruth Davee Department of Neurology, Northwestern University Feinberg School of Medicine, 320 E. Superior St, Searle 6-523, Chicago IL 60611, Phone: 312-503-3933, Fax: 312-503-3950, jmazzulli@northwestern.edu.

CRediT Author Contributions: Conceptualization, I.S., J.R.M; Methodology, Validation, Formal Analysis, and Investigation, I.S., W.Y.W. F.Z., N.R.B., E.P., N. M., K.S., L.F., J.R.M., Writing – Original Draft, I.S. and J.R.M.; Writing – Review & Editing, I.S., W.Y.W. F.Z., N.R.B., E.P., N. M., K.S., L.F., J.R.M., Visualization, I.S. and J.R.M., Supervision, J.R.M., Project Administration, J.R.M., Funding Acquisition, J.R.M.

Declaration of Interests: JRM is a scientific co-founder of Lysosomal Therapeutics, INC.

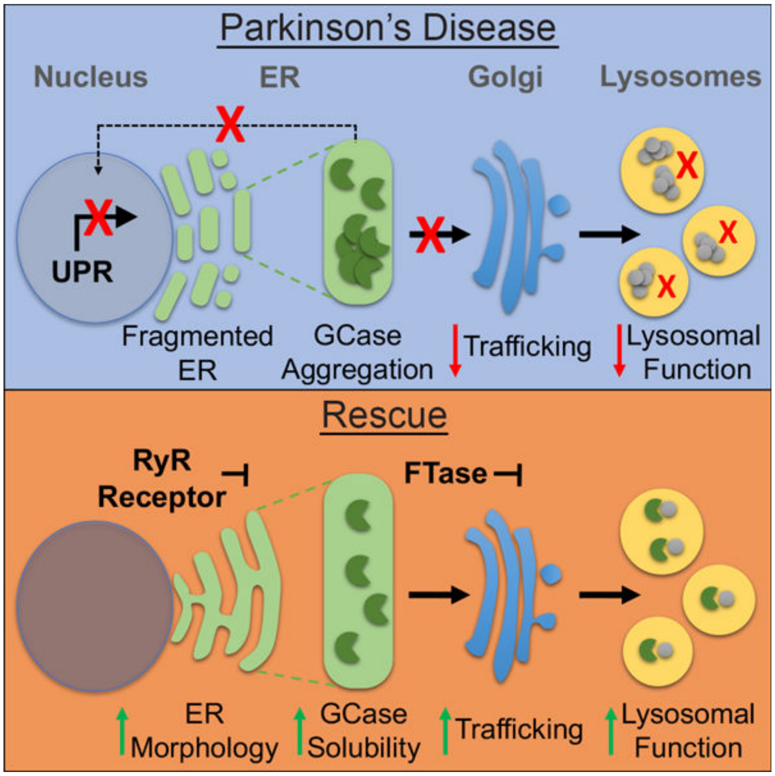

eTOC Blurb

Stojkovska et al. found that Parkinson's patient neurons accumulate α-synuclein and are deficient at recognizing misfolded proteins in the endoplasmic reticulum (ER), inducing pathogenic aggregation of immature lysosomal hydrolases. This phenotype is rescued by combined enhancement of ER proteostasis and protein trafficking, leading to lysosomal activation and reduction of a-synuclein.

Introduction

Parkinson's disease (PD) is characterized by the loss of dopaminergic neurons in the midbrain and the presence of protein inclusions called Lewy bodies and Lewy neurites that are comprised of α-synuclein (α-syn) (Spillantini et al., 1997). Critical to the pathogenic mechanism of α-syn, A53T and other familial-linked point mutations in *SNCA*, result in the accelerated oligomerization or fibrillization of the protein (Conway et al., 1998). Multiplications of wild-type *SNCA* also cause PD and the severity of their clinical phenotype is dependent on α-syn dosage. For example, the clinical presentation of *SNCA* duplication patients occurs much later and is not as severe as in *SNCA* triplications (Fuchs et al., 2007; Singleton et al., 2003). Patients with *SNCA* multiplications display the classical Lewy pathology, indicating that overabundance of the wild-type protein leads to neurodegeneration. However, our mechanistic understanding of how a-syn aggregates induce neurotoxicity is incomplete.

The presence of a-syn aggregates suggests that proteostasis pathways, including the lysosomal clearance pathway, are disrupted in the PD brain. Genome-wide association studies in PD patients have identified several risk genes, most of which have key roles in autophagy and lysosomal function (Chang et al., 2017; Nalls et al., 2014; Robak et al., 2017; Simon-Sanchez et al., 2009). Of these, loss-of-function mutations in *GBA1* represent one of the strongest genetic risk factors for the development of PD and Dementia with Lewy bodies (DLB) (Chia et al., 2021; Sidransky et al., 2009). Homozygous mutations in the *GBA1* gene, which encodes lysosomal β-glucocerebrosidase (GCase), cause the lysosomal storage disorder Gaucher's disease (GD) that is characterized by glycosphingolipid accumulation and neurodegeneration (Roshan Lal and Sidransky, 2017).

Genetic analyses indicate that defects in vesicular trafficking also contribute to PD pathogenesis (Abeliovich and Gitler, 2016; Hunn et al., 2015; Klein and Mazzulli, 2018; Martin et al., 2014; Singh and Muqit, 2020). Proper GCase maturation requires its trafficking from the endoplasmic reticulum (ER) to the Golgi portion of the secretory pathway. Previous work has shown that α-syn accumulation can impair ER-to-Golgi trafficking and disrupt protein maturation (Cooper et al., 2006; Gitler et al., 2008; Gosavi et al., 2002; Thayanidhi et al., 2010). Our recent studies showed that trafficking disruption occurs by α-syn-mediated inhibition of the SNARE protein ykt6, which prevents the fusion of ER-derived vesicles on the cis-Golgi causing downstream lysosomal depletion (Cuddy et al., 2019).

Perhaps the most critical function of the proteostasis network takes place in the ER compartment, where approximately one-third of the cell's proteome is synthesized, folded, and processed. Calcium-dependent molecular chaperones such as calnexin (CANX) are particularly important for maintaining proper protein folding and quality control of N-linked glycosylated proteins, including GCase and other lysosomal hydrolases (Ou et al., 1993; Tan et al., 2014). Disrupted protein trafficking and accumulation of immature proteins in the ER can overwhelm the folding machinery, leading to ER stress and initiation of the unfolded protein response (UPR). The UPR constitutes a series of pathways that transduce ER stress signals to the nucleus for transcriptional upregulation of quality control machinery and expansion of the ER to accommodate excess protein load (Walter and Ron, 2011). The three main UPR sensors include inositol-requiring enzyme (IRE1), double-stranded RNA-activated protein kinase (PKR)–like ER kinase (PERK), and activating transcription factor 6 (ATF6). Stimulation of these three branches acts to restore ER proteostasis by reducing protein synthesis and stimulating gene expression of folding machinery including chaperones GRP78 and GRP94 (Kozutsumi et al., 1988). *GBA1* mutations destabilize GCase structure, resulting in UPR induction, expansion of the ER compartment, and elimination of the protein through ER associated degradation (ERAD) (Fernandes et al., 2016; Garcia-Sanz et al., 2017; Ron and Horowitz, 2005). UPR activation has been documented in various synucleinopathy models including α-syn overexpressing yeast (Cooper *et al.*, 2006), A53T transgenic mice (Colla et al., 2012a; Colla et al., 2018), and iPSC-derived cortical neuron models (Chung et al., 2013; Heman-Ackah et al., 2017). Evidence of UPR activation has been shown in the substantia nigra of post-mortem PD brains (Credle et al., 2015; Heman-Ackah *et al.*, 2017; Hoozemans et al., 2007). Overexpression of the ER chaperone GRP78 can also reduce neurodegeneration in α-syn expressing animal models (Gorbatyuk et al., 2012), further emphasizing the importance of maintaining ER proteostasis in neuronal health. While these studies collectively suggest that ER dysfunction is associated with PD, the mechanistic link between α-syn accumulation, protein misfolding in the ER, and downstream lysosomal dysfunction has not been established. Furthermore, it is unknown whether enhancing ER proteostasis alone is sufficient to rescue lysosomal dysfunction and reduce pathological α-syn in PD patient neurons. To address these questions, we developed novel induced pluripotent stem cell (iPSC)-derived midbrain dopaminergic (DA) models from PD patients that carry a triplication (3X) in *SNCA*. We find that SNCA-3X patient neurons exhibit severe perturbations in the ER that lead to lysosomal dysfunction, and can be rescued by synergistic enhancement of protein folding in the ER and trafficking via small molecule modulators.

Results

Novel PD iPSC-derived midbrain models demonstrate α-syn accumulation and lysosomal dysfunction.

Our previous work indicated that α-syn accumulation causes lysosomal dysfunction in PD patient midbrain neurons (Cuddy *et al.*, 2019; Mazzulli et al., 2016b). To further examine the mechanism of this process, we generated and characterized new iPSC lines from controls (Ctrl) and three distinct patients that carry a triplication (3X) in *SNCA*, and exhibit early onset parkinsonism and dementia (Singleton *et al.*, 2003) (Figure S1 A–F). Select iPSC lines (termed 3x-1 (clone 3; C3), 3x-2 (clone 2; C2), 3x-4, and Ctrl (clone 1; C1) were differentiated into midbrain dopamine (DA) neurons (Kriks et al., 2011; Mazzulli *et al.*, 2016b), matured for 90 days, and analyzed for the presence of aggregated α-syn. Immunofluorescence and biochemical analysis indicated that patient lines accumulated insoluble α-syn within neurites and the cell body that were thioflavin positive compared to controls (Figure S2A–C). Analysis of GCase maturation by western blot showed a reduction in *SNCA*-3X DA neurons indicated by the accumulation of immature, low molecular weight forms of GCase (~55–62 kDa) (Figure 1A). We also observed a decline in GCase activity within lysosomal compartments of living *SNCA*-3X DA neurons (Figure 1B). Analysis of neurite degeneration by neurofilament immunostaining indicated no change at this time point, suggesting that the decline in activity is not due to cell toxicity (Figure 1C).

We next generated and characterized isogenic controls of *SNCA*-3X iPSC lines by targeted disruption of the *SNCA* gene using previously established CRISPR/Cas9 constructs (Zunke et al., 2018) (Figure S2D–F). We found a 50% decrease in *SNCA* expression in the 3x-1 isogenic control (Figure 1D), corresponding to a 70% decline in α-syn protein that is comparable to healthy controls (Figure 1E). Lines 3x-2 and 3x-4, exhibited a 75% reduction in *SNCA* mRNA (Figure 1D), and no detectable α-syn protein (Figure 1E). Moreover, no insoluble α-syn was detected in any of the isogenic control lines (Figure 1E). Analysis of DA neuron markers showed that α-syn reduction did not affect neural differentiation (Figure S2F), consistent with *in vivo* studies (Abeliovich et al., 2000). α-Syn reduction improved GCase maturation by reducing the accumulation of immature GCase, while promoting mature GCase (Figure 1F). Improved GCase maturation was validated by endoglycosidase

H (Endo H) digestion, which only cleaves glycans from immature GCase forms (Figure 1G), and increased lysosomal GCase activity (Figure 1H). These data validate previous findings in novel iPSC-derived synucleinopathy models, and indicate that wild-type GCase trafficking and activity is reduced by α-syn accumulation.

Immature GCase aggregates in the ER of patient midbrain neurons and synucleinopathy brains.

The accumulation of immature proteins in the ER can overwhelm the folding machinery, leading to protein misfolding (Marquardt and Helenius, 1992). Since immature forms of GCase accumulate in *SNCA*-3X DA neurons, we hypothesized that α-syn-induced trafficking disruptions may result in GCase instability, misfolding, and aggregation. To test this, lysates from *SNCA*-3X DA neurons were sequentially extracted and analyzed by western blot. We found that the proportion of aggregated, immature GCase in Triton X-100-insoluble fractions was elevated in *SNCA*-3X DA neurons compared to isogenic controls (Figure 2A). This was confirmed in a distinct synucleinopathy patient model expressing A53T α-syn that was previously characterized (Cuddy *et al.*, 2019) (Figure 2B).

To determine if insoluble GCase could occur from general perturbations in ER-Golgi trafficking that are independent of a-syn, we treated wild-type or isogenic control neurons with thapsigargin (Tg) to induce ER stress and perturb ER-Golgi trafficking. Although Tg induced ER stress as shown by increased GRP78 expression, we found no evidence of insoluble GCase accumulation (Figure S3A). Additionally, we assessed GCase aggregation in the brains of LIMP2 knock-out mice, since LIMP2 is required for ER-Golgi trafficking of GCase trafficking (Reczek et al., 2007; Rothaug et al., 2014). While the post-ER forms of GCase were depleted as expected, GCase did not accumulate but was instead depleted in LIMP2-/- mice (Figure S3B). This is consistent with previous studies showing that LIMP2 -/- reduces GCase levels through aberrant secretion. Collectively, our studies indicate that GCase accumulates into insoluble species selectively upon α-syn-induced inhibition of ER-Golgi trafficking, but not upon general ER stress induction or LIMP2 knock out.

To determine if GCase misfolds and aggregates *in vivo*, we compared the levels of GCase in 1% sarkosyl-insoluble fractions from brains of patients with either Dementia with Lewy bodies (DLB), or DLB with co-existing Alzheimer's disease (AD) pathology. In age-matched healthy control brains, we detected low levels of insoluble GCase that migrated at 55kDa likely representing the non-glycosylated immature protein, as well as GCase fragments that migrated between 42 and 48kDa (Figure 2C). Even though we observed some variability between control brains, comparison with age and post-mortem interval (PMI)-matched synucleinopathy brain showed a 1.8-fold elevation of insoluble GCase in DLB brain, and a more dramatic increase of nearly 4-fold in DLB+AD brain when normalized to total protein (Figure 2C, Table S1). Analysis of ER microsomes from idiopathic PD brain indicated that GCase aggregates occur in the ER *in vivo* (Figure 2D, Table S2). We also assessed the solubility of two additional hydrolases to address selectivity, including cathepsin D and hexosaminidase B. We found that insoluble immature forms of cathepsin D also accumulated in DLB brain, but hexosaminidase B was only found in the soluble fraction with no changes in the total levels observed between control and disease (Figure S3C, D,

Table S3). These data indicate that perturbations in maturation lead to the accumulation of aggregated, insoluble hydrolases in the ER of synucleinoapthy patient brain.

ER fragmentation in *SNCA*-3X DA neurons that accumulate immature wild-type GCase.

We hypothesized that accumulation of aggregated GCase in the ER would trigger the ER stress response. The UPR normally responds to misfolded proteins by expansion of the ER compartment and upregulation of ER chaperones to accommodate for the added protein load (Fujiwara et al., 1988; Schuck et al., 2009; Walter and Ron, 2011). Examination of ER morphology by electron microscopy indicated that *SNCA*-3X neurons unexpectedly did not exhibit ER expansion, but instead showed a decrease in total ER area relative to isogenic controls (Figure 3A), with shorter, fragmented ER tubules (Figure 3A). In contrast, Gaucher's disease (GD) neurons that express and retain mutant GCase in the ER (*GBA1* N370S/84GG) demonstrated a severely dilated ER, consistent with an activation of the UPR (Figure 3A). These data indicate that the ER fails to accommodate for the accumulation of misfolded, aggregated GCase by ER expansion, suggesting that *SNCA*-3X DA neurons may lack the ability to initiate a UPR response.

SNCA-3X DA neurons exhibit mild elevation of ER stress chaperones in the absence of UPR activation.

We next examined the levels of ER chaperones known to be involved in GCase folding or upregulated during ER stress including GRP78, GRP94, and calnexin (CANX) (Kozutsumi *et al.*, 1988; Tan *et al.*, 2014). GRP78 and GRP94 preferentially bind to misfolded or aggregated proteins with exposed hydrophobic patches (Marquardt and Helenius, 1992; Melnick et al., 1994), while CANX binds to monoglucosylated N-glycan branches of non-aggregated folding intermediates (Ou *et al.*, 1993) and retains them in the ER until properly folded (Rajagopalan et al., 1994). Compared to isogenic control lines, we observed a mild elevation in all three chaperones that ranged from 10–25% (Figure 3B). In comparison, GD-derived DA neurons carrying either the N370S/84GG or L444P/L444P mutation in GCase showed a more pronounced increase (~25–60%) in GRP78 and CANX relative to the healthy control, while GRP94 levels were elevated by ~25% only in the *GBA1* L444P/L444P mutant (Figure 3B). The increased levels of GRP78, GRP94, and CANX in GD neurons compared to *SNCA*-3X DA neurons are likely due to the destabilizing effect of the GCase mutations and are consistent with previous findings in fibroblast cultures (Ron and Horowitz, 2005).

The dramatic ER fragmentation phenotype and accumulation of aggregated immature GCase prompted us to examine UPR signaling pathways in more detail. We measured XBP1-S, a transcription factor that upregulates ER stress machinery upon IRE1 stimulation (Calfon et al., 2002; Yoshida et al., 2001), and the expression of its downstream transcriptional targets. Using two independent assays, we found no increase of XBP1-S in *SNCA*-3X DA neurons compared to controls (Figure S4A; Figure S4B, left). Moreover, the mRNA of GRP78 was reduced and CANX was not changed in *SNCA*-3X DA neurons, indicating the absence of UPR-induced transcriptional response (Figure 3C). To determine if the UPR could be triggered in *SNCA*-3X DA neurons by dramatic overexpression of misfolded GCase, we expressed the L444P mutant GCase by lentiviral infection. While expression of L444P

GCase induced an upregulation of GRP78 and GRP94 mRNA in control neurons, *SNCA*-3X DA neurons showed no response (Figure 3D). This indicates that PD patient neurons fail to sense or transmit misfolded protein stress signals to initiate the UPR.

We next determined if UPR could be activated in *SNCA*-3x DA neurons by established chemical ER stressors that induce the UPR through pleotropic effects. Tg and brefeldin A (BFA) activate the UPR through either disturbing calcium homeostasis, or directly block ER-Golgi trafficking machinery, respectively (Booth and Koch, 1989; Helms and Rothman, 1992; Price et al., 1992). We found that Tg and BFA induced an upregulation of XBP1-S (Figure S4B, right), and significantly increased mRNA / protein levels of ER chaperones in *SNCA*-3X DA neurons and α-syn overexpressing cell lines (Figure 3E; Figure S4C–F). XBP1-S mRNA and ER chaperone mRNA / protein levels were increased to a similar degree in both controls and *SNCA*-3x neurons (Figure 3E; Figure S4B, C, F). We next assessed the PERK pathway of the UPR by measuring eIF2α, a eukaryotic initiation factor which upon phosphorylation by PERK leads to global translational attenuation (Harding et al., 1999). We did not observe baseline elevation of phospho-eIF2α in patient neurons (Figure S4F), however treatment with Tg increased phospho-eIF2α to a similar degree in both isogenic controls and *SNCA*-3X DA neurons (Figure S4F). Collectively this indicates that while the UPR is capable of activation by chemical stressors that broadly activate the UPR, PD neurons are specifically deficient in recognizing and responding to misfolded proteins in the ER.

Misfolded proteins in the ER are normally recognized by quality control machinery and eliminated by ERAD, which is mediated by EDEM1 (ER degradation-enhancing α-mannosidase-like protein 1). EDEM1 is a lectin-containing adapter protein that removes misfolded glycoproteins from the CANX folding cycle and delivers them to the cytosol for proteosomal degradation (Smith et al., 2011) (Lee et al., 2003). We measured EDEM1 expression in *SNCA*-3X lines and found no change in mRNA or protein levels (Figure 4A–C). Since variability was observed in the levels of EDEM1 protein between culture samples of *SNCA*-3X lines, we correlated EDEM1 and α-syn protein levels in patient neurons and found a significant negative relationship (Figure 4D). This suggests that samples with abundant α-syn pathology have reduced EDEM1 levels and therefore compromised ERAD. Consistent with this, we found no change in the levels of wild-type GCase upon proteosomal inhibition of *SNCA*-3X DA neurons, suggesting that the protein is not cleared through ERAD (Figure 4E). In contrast, GD neurons showed a dramatic upregulation of EDEM1 compared to both healthy controls and *SNCA*-3X lines (Figure 4B, C), and significant elevation of GCase protein upon proteosomal inhibition (Figure 4F). These data indicate that despite retaining immature misfolded GCase in the ER, the EDEM1 / ERAD pathway is not activated in *SNCA*-3X DA neurons. In GD neurons, elevation of ERAD leads to elimination of mutant GCase.

α-Synuclein associates with ER chaperones in *SNCA*-3X DA neurons.

Although α-syn is known to be a synaptic protein under physiological conditions, immunofluorescence analysis indicated its accumulation at the cell body in *SNCA*-3X DA neurons (Figure S2A, B) (Cuddy *et al.*, 2019; Mazzulli *et al.*, 2016b). Studies in α-syn overexpression models also indicated that pathological α-syn can abnormally localize to the ER compartment (Bellucci et al., 2011; Colla *et al*., 2012a; Colla et al., 2012b; Colla *et al*., 2018; Guardia-Laguarta et al., 2014; Masliah et al., 2000; Paillusson et al., 2017). To determine if a-syn associates with the ER in *SNCA*-3X DA neurons, we used super-resolution imaging to examine the colocalization of a-syn with the established ER marker PDI, as well as enrichment of ER microsomes in neurons. We found that α-syn colocalizes with PDI in *SNCA*-3X patient neurons and is enriched within microsomal fractions (Figure S5A, B). In-situ proximity ligation assays (PLA) and co-immunoprecipitation in α-syn overexpressing cell lines showed that α-syn associates with CANX and GRP94 (Figure 5A, B; Figure S5C). PLA analysis validated that endogenously expressed α-syn associates with ER chaperones CANX and GRP94 in SNCA 3X neurons more than controls (Figure 5C). Together, these results suggest that α-syn may disrupt ER proteostasis and GCase trafficking through aberrant association and sequestration of ER chaperones.

Synergistic activation of ER proteostasis and trafficking rescues lysosomal function and reduces α-syn.

We next determine if increasing ER chaperone function could rescue lysosomal GCase activity. Previous studies showed that ER proteostasis in GD can be improved by blocking ryanodine receptors (RyRs) that mediate calcium efflux from the ER, thereby increasing CANX function (Mu et al., 2008; Ong et al., 2010; Sun et al., 2009). We selected the RyR inhibitor diltiazem (DILT), since it is an FDA-approved treatment for high blood pressure and angina. Treatment of *SNCA*-3X neurons with 25μM DILT abrogated the build-up of insoluble GCase while concomitantly elevating soluble GCase starting at 2 weeks and continuing to 8 weeks of treatment (Figure 6A). Although DILT mainly increased the solubility of immature forms of GCase, we observed a slight elevation in post-ER forms, indicating a mild improvement in maturation (Figure 6B). DILT also improved GCase protein levels and maturation in control DA neurons, suggesting that enhancement of the folding pathway can be achieved in neurons under physiological conditions (Figure S6A). DILT enhanced properly folded, functional GCase, as demonstrated by increased GCase activity in whole cell lysates that include both ER and post-ER forms (Figure 6C, left). Despite this, the *in situ* assay that measures GCase activity within lysosomes of living neurons indicated no change, and western blot showed that or a-syn was also unchanged (Figure 6C right, 6D). We validated that DILT could enhance chaperone function in patient neurons by measuring the binding activity of CANX to N-glycosylated proteins using the lectin concanavalin A (Con-A) (Figure 6E). Taken together, these results suggest that enhancing ER proteostasis with DILT can promote functional, soluble forms of GCase, but cannot improve lysosomal function in a sufficient manner to reduce α-syn.

To confirm that enhancing ER proteostasis and wild-type GCase can be improved by RyR inhibition, we treated α-syn overexpressing cell lines and *SNCA*-3X DA neurons with two additional RyR inhibitors, dantrolene (DANT) and 1,1′-diheptyl-4,4′-bipyridinium (DHBP) (Fruen et al., 1997; Kang et al., 1994). DANT and DHBP treatment elevated soluble GCase levels in cell models, although not as robustly as DILT (Figure S6B–D). When higher concentrations or longer incubation periods were attempted, we observed cell toxicity, consistent with previous findings (Ong *et al*., 2010; Wang et al., 2011). We confirmed that improved GCase solubility occurred through RyR3 by knock-down with shRNA constructs. RT-PCR analysis showed a 50% knock-down (KD) of RyR3 (Figure S6E), resulting in increased solubility of GCase in both cell lines and *SNCA*-3X DA neurons (Figure 6F; Figure S6F). DILT had no effect on GCase solubility in RyR3 KD cells (Figure S6F), indicating that DILT acts to improve GCase through RyR3 receptors on the ER. Analysis of GCase maturation in RyR3 KD cells showed a mild improvement in cell lines similar to DILT treatment, and no change in *SNCA*-3X DA neurons (Figure 6F; Figure S6F). DILT caused a mild elevation of GCase maturation in RyR3 KD cell lines, a result that may have occurred from the inhibition of other RyR isoforms (Figure S6F). These data show that RyR inhibition can improve GCase proteostasis in the ER, but has little effect on increasing GCase trafficking in patient neurons.

The failure to rescue lysosomal GCase activity by RyR inhibition suggests that factors downstream of the ER may inhibit hydrolase trafficking. Our previous work showed that α-syn inhibits GCase trafficking by preventing ER-Golgi vesicle fusion through impeding the function of the SNARE protein ykt6 (Cuddy *et al.*, 2019). Further, farnesyltransferase inhibitors (FTIs) can restore ykt6 activity, thereby improving GCase trafficking and lysosomal activity in PD neurons (Cuddy *et al.*, 2019). Therefore, we next determined whether enhancing trafficking, together with ER proteostasis, could cooperate to rescue lysosomal GCase. We found that treatment with the FTI (LNK-754) and DILT resulted in a significant increase of GCase maturation compared to each compound alone (Figure 7A, Figure S7A–C). This effect was not additive but synergistic, since the increase caused by FTI + DILT was greater than the sum of each individual compound alone at 4 weeks of treatment (Figure S7A). This is consistent with the notion that each compound targets a distinct portion of the proteostasis pathway. EM analysis indicated that FTI + DILT treatment substantially improved ER segment length and area, suggesting that increased movement of GCase out of the ER improves ER morphology (Figure 7B). FTI + DILT treatment also elevated functional, soluble forms of GCase in both whole cell lysates and live-cell *in situ* lysosomal assays (Figure 7C) and synergistically reduce both soluble and insoluble α-syn in patient neurons and cell lines (Figure 7D, E; Figure S7B–D). We confirmed our findings genetically, by combining RyR3 KD with FTI, or DILT with expression of ykt6-CS that cannot be farnesylated (Cuddy *et al.*, 2019). These combinations effectively enhanced GCase trafficking and reduce α-syn better than either treatment alone (Figure S7E–H). Finally, we sought to determine if the combination treatment could improve GCase proteostasis and reduce α-syn levels in patient iPSC neurons that express *GBA1* mutations. FTI+DILT treatment of GD midbrain neurons (N370S / 84GG) and a GBA-PD patient (N370S / wt) significantly increased GCase maturation and reduced α-syn levels compared to each treatment alone (Figure S8). This suggests that combined trafficking and ER proteostasis enhancers could provide benefit in both synucleinopathies and GD.

Discussion

We identify a novel pathogenic pathway induced by a-syn accumulation at the ER characterized by severe ER fragmentation, compromised folding capacity, and aggregation of lysosomal GCase (Figure 8). Other studies using transgenic overexpression models of α-syn have documented the association of α-syn with ER components (Colla *et al.*, 2012a), and are consistent with our findings in PD patient neurons. Our data indicates that a-syn likely interacts with ER chaperones that are important for maintaining GCase folding (Figure 5; Figure S5). It is possible that the interaction occurs from increased abundance of α-syn at the cell body. However our previous studies have shown that a-syn does not interact with other ER-Golgi components located at the cell body (Cuddy *et al.*, 2019; Mazzulli et al., 2016a), suggesting that the ER chaperone association is somewhat selective. Increased α-syn at the ER may overwhelm the proteostasis capacity sequestering chaperones away from their normal function. α-Syn can also directly perturb protein trafficking machinery downstream at the Golgi (Cuddy *et al.*, 2019; Gitler *et al.*, 2008), which likely slows the export of cargo from the ER, resulting in the accumulation of immature proteins. These data highlight the negative effects of α-syn on multiple branches of the proteostasis pathway.

A surprising consequence of α-syn-induced trafficking disruption was the aggregation of immature GCase into insoluble species (Figure 2). While several loss of function mutations in lysosomal hydrolases can cause lysosomal storage diseases (Zunke and Mazzulli, 2019), we document a unique example where lysosomal dysfunction occurs through the misfolding and aggregation of wild-type immature GCase. Other lysosomal diseases that are caused by mutations in trafficking machinery including I-Cell disease, or LIMP2 depletion that occurs in acute myoclonus renal failure (AMRF), do not show accumulation of immature hydrolases but instead are characterized by aberrant secretion (Figure S3B) (Reczek *et al.*, 2007; Wiesmann et al., 1971). Therefore, the aggregation of immature hydrolases induced by a-syn may be unique to synucleinopathies. The lack of chaperone induction and ERAD activity in *SNCA*-3X DA cultures (Figure 4) likely contributes to the aberrant accumulation and destabilization of GCase in the ER. GCase may also be particularly susceptible to aggregation as a membrane-associated enzyme, since aberrant exposure of hydrophobic patches during prolonged folding cycles may promote its self-association into insoluble aggregates. We also found that immature cathepsin D accumulates into insoluble species, but not hexosaminidase B (Figure S3). This indicates that while not all hydrolases are susceptible to aggregation, the effect is not specific for GCase. One other study has shown that a rare Tay-sachs disease point mutation in β-hexosaminidase results in the accumulation of an insoluble enzyme precursor, preventing its trafficking to the lysosome (Proia and Neufeld, 1982). It will be of interest in future studies to examine hydrolase aggregation in proteinopathies beyond PD and DLB, that are characterized by lysosomal dysfunction.

Unexpectedly, we did not observe activation of the UPR in *SNCA*-3x neurons, which normally prevents protein aggregation by expanding ER volume and upregulating folding machinery. Other synucleinopathy models generated by transgenic α-syn overexpression or patient-derived iPSC cortical models exhibited signs of UPR activation (Colla *et al.*, 2012a; Heman-Ackah *et al.*, 2017). The pathological stage at which the models were examined is an important consideration. In some studies, ER stress markers are only elevated during the latest stages of pathology (Colla *et al.*, 2012a; Credle *et al.*, 2015; Heman-Ackah *et al.*, 2017; Hoozemans *et al.*, 2007) which may be a general characteristic of late-stage, age-related diseases (Wang and Kaufman, 2016). We focused on the early stages of disease to capture phenotypic events that occur prior to lysosomal dysfunction and neurodegeneration. Our findings suggest that PD neurons are deficient at detecting and responding to misfolded proteins (Figure 8), as indicated by lack of UPR induction after overexpression of L444P

GCase in *SNCA*-3X neurons. Conversely, activation of the UPR occurs in GD neurons that endogenously express mutant GCase, or in wildtype neurons that overexpression of L444P, demonstrating that the UPR sensors are capable of detected misfolded GCase. Therefore, it is likely that α-syn impedes the ability of the UPR sensors to detect misfolded GCase, or downstream signal transduction required to activate UPR genes. While patient neurons could not respond to misfolded GCase, they could react to chemical ER stress inducers that induce non-specific, pleiotropic effects on the UPR. This indicates that while UPR pathway is not completely disabled, *SNCA*-3x neurons exhibit a selective deficiency in handling misfolded proteins in the ER. The mechanisms that conceal folding status in the ER require further study, but may involve aberrant interactions of a-syn with ER chaperones and stress sensors.

Recent work has shown that the UPR can be harnessed to provide protection in neurodegenerative diseases (Grandjean et al., 2020; Vidal et al., 2021). Since our data indicates that the UPR is not completely disabled, it is possible that enhancing the pathway will provide therapeutic benefit. Such strategies could restore ER proteostasis by stimulating XBP1-S-mediated ER compartment expansion and elevation of chaperones, providing a more conducive environment for GCase folding while preventing the growth of GCase aggregates. These methods would have to avoid maladaptive UPR signaling pathways that promote apoptosis from prolonged stimulation (Wang and Kaufman, 2016).

Our rescue studies indicate that current therapeutic strategies focused on enhancing single branches of the proteostasis pathway may be insufficient to completely rescue PD pathology. Previous work from our group and others showed that FTIs can enhance trafficking and activate lysosomes, reducing aggregated proteins *in vivo* (Cuddy *et al.*, 2019; Hernandez et al., 2019). Our current work indicates that combining this strategy with ER proteostasis enhancers is more efficient at rescuing lysosomal GCase and reducing pathological α-syn (Figure 7, Figure S7). Once in the lysosome, active GCase could reduce α-syn by degrading glycosphingolipid substrates that interact and stabilize toxic α-syn (Zunke *et al.*, 2018). This strategy was also effective in patient neurons that harbor *GBA1* mutations (Figure S8), indicating a potential to translate these treatments to GD and GBA-PD. Therapeutic enhancement of multiple proteostasis pathways may provide optimal benefit in PD, given the pleiotropic deleterious effects of α-syn accumulation in multiple subcellular locations. Furthermore, combining two treatments that target distinct cellular pathways may enable administration of lower doses of each drug, which would limit compound toxicity if these treatments should progress to the clinic.

STAR METHODS

RESOURCE AVAILABILITY

Lead Contact—Further information and requests for resources and reagents should be directed to and will be fulfilled by the Lead Contact, Joseph R Mazzulli (jmazzulli@northwestern.edu).

Materials Availability—All unique/stable reagents and cell lines generated in this study are available from the Lead Contact, Joseph R Mazzulli (jmazzulli@northwestern.edu) with a completed Materials Transfer Agreement.

Data and Code Availability

- Data availability: All data reported in this paper will be shared by the lead contact upon request.
- Code: This paper does not report original code
- Any additional information required to reanalyze the data reported in this paper is available from the lead contact upon request.

EXPERIMENTAL MODEL AND SUBJECT DETAILS

Human H4 neuroglioma cell culture—Human H4 neuroglioma cells were stably transfected to overexpress wild-type α-syn under the control of a tetracycline-inducible promoter via a Tet-off system and described previously (Mazzulli et al., 2011). α-Syn expression was turned off by the addition of 1ug/ml doxycycline (DOX) (Sigma), a tetracycline analog, for a minimum of 3 days. Cells were cultured in Optimem media with 5% heat-inactivated FBS, 0.2 mg/ml geneticin, 0.2 mg/ml hygromycin B, and 1% penicillin / streptomycin (Thermo Fisher Scientific).

iPSC model generation, characterization and culture methods

Reprogramming and culturing of human induced pluripotent stem cells (iPSCs): B-lymphocytes from healthy controls and PD patients that carry a triplication in the *SNCA* genomic region were obtained from the Coriell NINDS and NIGMS Human Genetic Cell Repositories: GM15845 (Ctrl), GM15010 (3x-1), ND00196 (3x-2), ND00139 (3x-4), ND34391 (Est. 3X). Phenotypic and genotypic data of these subjects is available on https://www.coriell.org. See Key Resources Table for more details, including information on Est. Ctrl, *SNCA* A53T mutant, and *GBA1* mutant iPSC lines (N370S/84GG and L444P/L444P). The B-lymphocytes were reprogrammed into iPSCs by transfection with non-integrating episomal plasmids containing Oct3/4 (Addgene: pCXLE-hOCT3/4-shp53-F), L-Myc (Addgene: pCXLE-hUL), and Sox2 and Klf4 (Addgene: pCXLE-hSK). All iPSCs were maintained in mTeSR1 media on matrigel-coated plates.

Pluripotency analysis of reprogrammed iPSC cells

I. Immunofluorescence analysis of pluripotency markers: Cells plated on glass coverslips were fixed in 4% paraformaldehyde (Polysciences, Inc.) for 15 minutes, permeabilized with 0.3% Triton X-100 (Sigma) in PBS for 30 minutes, and blocked with 2% bovine serum albumin (BSA) (Roche) in Triton-PBS for 30 minutes to prevent non-specific antibody binding. Primary antibodies (Sox2, Tra-1–60, Oct4, SSEA4, Nanog) were added overnight, followed by incubation with secondary antibodies (Alexa Fluor 488 Goat anti-rabbit IgG and Alexa Fluor 568 Goat anti-mouse IgG) for 1 hour. The cells were then washed three times with Triton-PBS and mounted onto microscope slides with DAPI mounting media.

II. PCR analysis of reprogramming factor transgenes: Forward and reverse PCR primers for each of the reprogramming factor transgenes (Oct3/4, Sox2, Klf4, L-Myc) were designed so that the PCR product will span both the transgene and the plasmid backbone, as indicated in the schematic of Figure S1C. See Table S4 for list of primers. The PCR was performed with Taq polymerase (NEB #M0273L) and 20ng of genomic DNA using the following cycling conditions : Initial denaturation 95 C 3min; 40 cycles : Denaturation 95C 30s, Annealing 60C 30s, Extension 68C 30s; Final extension 68C 5min; 4C hold. The PCR products were run on 1.5% agarose gel for 45min at120V and imaged on a Chemicdoc imaging system (Biorad).

Quantitative RT-PCR: Total RNA was isolated from cells in a 24 or 12 well format using an RNeasy Mini Prep kit (QIAGEN). cDNA was synthesized by reverse transcriptase PCR (RT-PCR) using the RevertAid First Strand cDNA synthesis kit (Thermo Fisher Scientific). Quantitative PCR was performed on the Applied Biosystems 7500 Fast system using the cDNA and pre-designed TaqMan-primer probes for the target genes. The target mRNA expression was quantified relative to GAPDH or β-actin using the delta-delta-Ct method, and represented as a fold change.

Copy number analysis of SNCA and puromycin: Genomic DNA was extracted from a 12 well plate of iPSCs using the DNeasy Blood and Tissue Kit (69504, Qiagen). Quantitative PCR was performed using default cycling conditions on the Applied Biosystems 7500 Fast system with 100ng genomic DNA and pre-designed TaqMan probe for SNCA (Hs04791950_cn) or custom probe for puromycin (gi763524_CCN1F1Y). The copy number of each gene was quantified relative to reference RPPH1 copy number assay (4401631, Applied Biosystems). The analysis was performed using ddCt method and expressed as fold change.

Fluorescence in-situ hybridization (FISH) analysis: To confirm the *SNCA* copy number in the reprogrammed iPSCs, fluorescent probes targeting *SNCA* (4q22.1; R: red) and a control region (4p16.3; G: green) were used for FISH analysis. The assay was performed as a service provided by Cell Line Genetics, Inc (www.clgenetics.com).

Differentiation of iPSCs into midbrain dopaminergic neurons: The iPSCs were differentiated into midbrain dopaminergic neurons using a well-established dual SMAD inhibition protocol (Kriks *et al.*, 2011), and have been previously described in detail (Mazzulli *et al.*, 2016a). Neurons were cultured in neurobasal SM1 media (Thermo Fisher Scientific) containing NeuroCult SM1 supplement (StemCell Technologies), 1% penicillin / streptomycin, and 1% L-glutamine (Gibco). Neurons were aged to 60–90 days for each experiment as indicated in the text or figure legends.

Dual nickase CRISPR/Cas9 strategy and selection of iPSC clones: A pair of guide RNAs (guide RNA 1: 5'-AGCAGCCACAACTCCCTCCTTGG-3'; guide RNA 2: 5'-TGAGAAAACCAAACAGGGTGTGG-3') were designed using the Optimized CRISPR design tool (http://crispr.mit.edu/), and used to direct D10A mutant Cas9 to produce nicks within Exon 2 of the *SNCA* gene. A PITX3–2A-eGFP-PGK-Puro plasmid (Addgene) encoding a puromycin resistance cassette driven by a phosphoglycerate kinase (PGK) promoter was used as a template for homologous recombination (HR) and as a positive selection marker. The gRNAs were cloned into a Cas9-nickase plasmid PX335 (Addgene) and transfected into iPSCs using Lipofectamine 3000 (Thermo Fisher Scientific) along with a puromycin-containing HR plasmid. Two days following the transfection, iPSCs were cultured in 1ug/ml puromycin containing media for several weeks. To confirm that the puromycin cassette was appropriately inserted in the targeted *SNCA* Exon 2 region, puromycin resistant clones were selected and genomic DNA was extracted and analyzed via PCR using the following primers: 5’ F: CATAAAATCTGTCTGCCCGCTCTC, 5’ R: GTGGGCTTGTACTCGGTC; 3’ F: CTTCTACGAGCGGCTCGGCTT, 3’ R: TGTGGTCATCCTCCACCTGACT. Puromycin copy number analysis and sequencing were also performed on selected clones.

Analysis of off-target effects using the T7EI cleavage assay: Genomic DNA was amplified using primers for each off-target gene (see Key Resource Table for list of primers). The PCR products were then denatured and allowed to re-anneal using a thermal cycler with the following settings: 95°C for 10 minutes, 95–85°C (ramp rate 2°C/sec), and 85–25°C (ramp rate 0.2°C/sec). The hybridized product was then digested with T7 Endonuclease I for 1 hour at 37°C, and analyzed on an agarose gel along with a positive control (Genecopoeia).

METHODS DETAILS

Biochemistry and Molecular Biology

Sequential protein extraction and western blotting analysis: Cells were harvested in 1X PBS and pelleted by centrifugation at 400xg for 5 minutes. The cell pellets were extracted via homogenization in 1% Triton lysis buffer containing protease inhibitor cocktail (PIC) (Roche), phenylmethylsulfonyl fluoride (PMSF) (Sigma), sodium orthovanadate (Na_3VO_4) (Sigma) and sodium fluoride (NaF) (Sigma). The Triton extracted lysates were freeze-thawed three times and ultracentrifuged at 100,000xg for 30 minutes at 4°C. The Triton-insoluble pellets were further extracted in 2% SDS lysis buffer containing PIC via boiling for 10 minutes, followed by sonication and then ultracentrifugation at 100,000xg for 30 minutes at 22°C. The protein concentrations of the Triton and SDS fractions were measured via a BCA protein assay kit (Thermo Fisher Scientific) on a plate reader. Extracted protein lysates were boiled in 1X Laemmeli sample buffer containing 2% SDS, loaded on an SDS-PAGE gel, transferred onto a PVDF membrane (Millipore), and post-fixed in 0.4% paraformaldehyde. Membranes were blocked in a 1:1 mixture of 1X TBS and Intercept blocking buffer (Li-Cor Biosciences), followed by overnight incubation with primary antibodies diluted in a 1:1 mixture of 1X TBS-Tween and blocking buffer. The following day, secondary antibodies were added for 1 hour, and the membranes were scanned using a Li-Cor Biosciences infrared imaging system. Quantification of band intensity was done using the ImageStudio software and analysis was performed on Excel and GraphPad Prism. A detailed protocol of this procedure has been published (Stojkovska and Mazzulli, 2021). In some blots, irrelevant lanes were cropped out, which is indicated by a dotted line or white space between the lanes.

To quantify insoluble GCase from cell cultures, the intensity from the soluble and insoluble fractions (using Sigma antibody G4171) was normalized to total protein obtained from the Coomassie blue stained gel of the corresponding membrane. Normalized intensities of soluble and insoluble fractions were added to obtain the total GCase signal. The % insoluble GCase was calculated by dividing the insoluble intensity by the total multiplied by 100, then expressed as fold change compared to the control lines or vehicle treated samples. The proportion of insoluble GCase in healthy wild-type cells ranged between 10–20%. For diltiazem treatment, quantification for the 2-week treatment is combined from day 90 3x-1 (n=6) and 3x-2 (n=3) neurons; 8-week treatment is of day 120 3x-1 neurons only (n=3). For human brain extracts, see below under "Insoluble hydrolase analysis of synucleinopathy brain tissues."

Co-immunoprecipitation: H4 cells overexpressing a-syn were extracted in 0.3% CHAPS buffer containing 40mM HEPES pH 7.4, 120mM NaCl, 1mM EDTA, 10% vol/vol glycerol, protease inhibitor cocktail (PIC) (Roche), phenylmethylsulfonyl fluoride (PMSF) (Sigma), sodium orthovanadate (Na_3VO_4) (Sigma) and sodium fluoride (NaF) (Sigma). 1mg of total lysate was pre-cleared with normal mouse IgG (Santa Cruz) and protein A/G beads that were blocked in 2% BSA. Pre-cleared lysates were incubated with 3ug of CANX antibodies (clone E-10, Santa Cruz) or 3ug of normal mouse IgG rotating end over end, overnight at 4°C. Blocked protein A/G beads were added and incubated for an additional 2 hours, followed centrifugation at 1000 X G, washing 3 times in CHAPS buffer, and elution by boiling in 2X Laemmeli sample buffer. The samples were analyzed by western blot as described above.

Sequential extraction analysis of LIMP2 knock-out mice: LIMP2 knock-out mice have been previously described and characterized (Rothaug et al., 2014). Brain tissue was sequentially extracted as described for cell cultures in "Sequential protein extraction and western blotting analysis". An additional extraction step was added for both Triton and SDS steps to avoid carry over between the fractions. Protein assay was performed by BCA, and 40ug of total protein was loaded per well. GCase solubility was assessed using the anti-GCase antibody from Sigma (G4171), and normalized to total protein obtained from Coomassie blue stained gels of the corresponding membranes.

Live-cell lysosomal GCase activity assay: The procedure and analysis method for the activity assay has been previously described in detail (Cuddy and Mazzulli, 2021) Briefly, cells were plated in 96-well plates. One day prior to the assay, cells were treated with 1mg/ml cascade dextran blue (Life Technologies) for 24 hours. The next day, the cells were first treated with DMSO or 200nM bafilomycin A1 (Santa Cruz) for 1 hour at 37°C, followed by a 1 hour pulse-chase with 100ug/ml artificial fluorescent GCase substrate, 5-(pentafluoro-benzoylamino) fluorescein di-ß-D-glucopyranoside (PFB-FDGluc) (Life Technologies), at 37°C. The fluorescence signal was measured every 30 minutes for the span of 3–4 hours on a plate reader (Ex=485nm, Em=530nm, for the GCase substrates; Ex=400nm, Em=430nm for cascade dextran blue). For the analysis, the GCase fluorescence signal was normalized to either lysosomal mass by using cascade dextran blue signal or total cell volume by quantifying CellTag 700 staining signal.

In vitro whole-cell lysate GCase activity assay: The procedure and analysis method for the activity assay has been previously described in detail (Mazzulli *et al.*, 2011). Briefly, 1% BSA and 5ug of Triton-soluble protein lysate treated with or without conduritol-β-epoxide (CBE, an inhibitor specific for lysosomal GCase) (Millipore) were added to GCase activity assay buffer (0.25% w/v sodium Taurocholate, 0.25% TritonX-100, 1mM EDTA, into a citrate/phosphate buffer pH 5.4) to a final volume of 100ul in a 96-well black bottom plate. The samples were incubated with 5mM fluorescent GCase substrate 4-methylumbelliferyl β-glucopyranoside (4-MU-Gluc) (Chem-Impex) for 30 minutes at 37°C, and the reaction was stopped using equi-volume of 1M glycine, pH 12.5. The fluorescence signal was measured on a plate reader (Ex=365nm, Em=445). Relative fluorescence units from CBE treated lysates were subtracted from non-CBE treated lysates to obtain the activity of GCase.

Endoglycosidase H (Endo H) digestion: These methods have been described in detail previously (Cuddy and Mazzulli, 2021). To study the subcellular localization and trafficking of GCase between the ER and Golgi, we digested protein lysates with Endoglycosidase H (Endo H) (New England Biolabs). The experimental procedure was performed according to the manufacturer's instructions. Briefly, 10X Glycoprotein Denaturing buffer was added to 40 μg of protein and the reaction was boiled at 100°C for 10 minutes. Following the denaturation, 10X GlycoBuffer 3 and Endo H enzyme were added, and the reaction was incubated at 37°C for 2 hours. Finally, the samples were boiled at 100°C for 10 minutes after the addition of 5X Laemmli buffer and loaded on a 10% SDS-PAGE gel, followed by western blot analysis. A positive digestion results in a downward shift in the molecular size of GCase after it is subjected to SDS-PAGE. Post-ER (70–74 kDa) and ER (55 kDa) forms of GCase were analyzed using the Endo H digested lane, and used as a measure of GCase trafficking.

Insoluble hydrolase analysis of synucleinopathy brain tissues: Sequential protein extraction was performed on post-mortem frontal cortex brain tissues (obtained from the Northwestern University Alzheimer's disease pathology core) obtained from controls, DLB, and DLB+AD patients. We employed a 5-step extraction protocol using high salt buffer, 1% Triton X-100, 1% Triton + 30% sucrose (Sigma), 1% sarkosyl (Sigma), and sarkosyl-insoluble extracts. Brain tissues were homogenized in high-salt buffer (HSB) (50 mM Tris-HCl pH 7.4, 750 mM NaCl, 10 mM NaF, 5 mM EDTA) with protease and protein phosphatase inhibitors, incubated on ice for 20 minutes and centrifuged at 100,000 x g for 30 minutes at 4 °C. The pellets were then re-extracted with HSB, followed by sequential extractions with 1% Triton X-100-containing HSB and 1% Triton X-100-containing HSB with 30% sucrose. The pellets were then resuspended and homogenized in 1% sarkosyl-containing HSB, rotated at 4 °C overnight and centrifuged at 100,000 x g for 30 min. The resulting sarkosyl-insoluble pellets were washed once with PBS and resuspended in PBS by brief sonication. This suspension was termed the 'sarkosyl-insoluble fraction', which was analyzed by western blot. GCase was probed using Sigma antibody G4171, and the total intensity of the immunoreactive signal from *ca*. 45kDa to 60kDa was normalized to Coomassie blue staining of the corresponding gel.

Insoluble GCase analysis of ER microsome-enriched idiopathic PD brain tissues: ER microsomes were enriched using subcellular fractionation and the purity of the fractions have been assessed previously (Mazzulli *et al*., 2011). Post-mortem cingulate cortex brain tissues obtained from idiopathic PD patients were lysed and homogenized in 0.25M sucrose buffer containing 10mM HEPES (pH 7.4) and 0.01M EDTA, and centrifuged at 6,800 x g for 5 minutes at 4°C to remove nuclei and unbroken cells. The extraction was repeated to wash the pellet. The final supernatants were combined and further centrifuged at 17,000 x g for 10 minutes at 4°C to remove mitochondria. Further centrifugation of the resulting supernatant at 100,000 x g for 1 hour was done to pellet the ER microsome components. Sequential extraction of soluble and insoluble protein from this final pellet was performed using 1% Triton and 2% SDS lysis buffer, respectively, as described above. Insoluble fractions were analyzed via western blot. GCase was probed using Sigma antibody G4171, and the total intensity of the immunoreactive signal shown (from *ca.* 50 to 64kDa) was normalized to Coomassie blue staining of the corresponding gel.

GBA1 mutation genotyping of human brain samples: Genomic DNA was extracted from 50mg human brain tissue (frontal / temporal cortex) using the PureLink genomic DNA kit (Invitrogen). To amplify the *GBA1* gene, 25ng genomic DNA was used as a template for PCR using the following forward and reverse primers, respectively: 5'-TGTGTGCAAGGTCCAGGATCAG-3' and 5'-ACCACCTAGAGGGGAAAGTG-3'. The PCR products were run on a 1% agarose gel to confirm amplification of the *GBA1* gene and to rule out accidental amplification of the *GBA1* pseudogene (*GBAP*). Sequencing of the most common *GBA1* mutations (L444P, N370S, E326K) was performed using primers listed in the Key Resource Table, and analysis was done using the Snapgene software.

ER microsome-enrichment of iPSC-derived neurons: ER microsomes were enriched using subcellular fractionation. *SNCA*-3X and healthy and isogenic control iPSC-derived neurons were gently homogenized in sucrose HEPES buffer (SHB). The homogenate was centrifuged at 6,800 x g for 5 minutes at 4C to remove nuclei and unbroken cells. Following removal of the supernatant (S1), the extraction was repeated using SHB buffer and the second supernatant (S2) was combined with S1. The combined supernatants (S1+S2) were further centrifuged at 17,000 x g for 10 minutes at 4C to remove mitochondria. Further centrifugation of the resulting supernatant (S3) at 100,000 x g for 1 hour at 4C removes the cytosolic components (supernatant S4), leaving the ER microsomes in the third and final pellet, termed P3. The P3 pellet was extracted in 1% Triton lysis buffer and analyzed by western blot.

Semi-quantitative RT-PCR analysis of XBP1 mRNA: Using cDNA as the template, human XBP1 mRNA was detected using PCR primers (forward: TTACGAGAGAAAACTCATGGCC; reverse: GGGTCCAAGTTGTCCAGAATGC) specific for both spliced (S; product size 263 bp) and unspliced (U; product size 289) isoforms. The PCR product was analyzed on an agarose gel along with a brefeldin A positive control.

Assessment of calnexin activity by Concanavalin-A pulldown: H4 neuroglioma cells were treated with vehicle or 25uM Diltiazem (Sigma) for 4 days, harvested, and extracted in 0.3% CHAPS lysis buffer (0.3% CHAPS, 40mM HEPES pH 7.4, 120 mM NaCl, 1mM EDTA, 10% v/v glycerol). For pulldown of total N-linked glycosylated proteins, 1500 µg lysate was mixed with 20 µg/ml biotinylated Concanavalin A (CON-A) (Vector Laboratories) and the reaction mixture was incubated overnight at 4°C under gentle rotation.

To recover CON-A bound proteins, 25 μl neutrAvidin agarose beads (Thermo Fisher Scientific) were added to the reaction mix and samples were incubated at 4°C for 1 hour. The beads were collected by centrifugation at 2500 x g for 2 min, followed by three washes with lysis buffer. N-glycosylated proteins were eluted by boiling the samples at 95°C for 10 min in 2X Laemmli sample buffer. Samples were analyzed by western blot for calnexin (CANX), GCase, and total N-glycosylated proteins by Coomassie brilliant blue staining. Calnexin activity was indirectly assessed by quantifying CANX levels in CON-A pulled down samples.

Imaging analysis

Immunofluorescence analysis of midbrain neuron differentiation efficiency, α-synuclein accumulation, and thioflavin staining: Neurons were fixed in 4% paraformaldehyde for 15 minutes, permeabilized with 0.1% Triton X-100 in PBS for 30 minutes, and blocked with 2% BSA and 5% normal goat serum (NGS) (Jackson Immuno Research) in Triton-PBS for 30 minutes to prevent non-specific antibody binding. Primary antibodies (anti-α-synuclein LB509, anti-tyrosine hydroxylase (TH), anti-FoxA2, anti-β3-tubulin) were added overnight, followed by incubation with secondary antibodies (Alexa Fluor 488 Goat anti-mouse IgG and Alexa Fluor 568 Goat anti-rabbit IgG) for 1 hour. The cells were then washed three times with Triton-PBS and mounted onto microscope slides with DAPI mounting media. For thioflavin S (Thio S) co-staining, following primary incubation with a-syn, 0.05% Thio S was directly added to cells and incubated for 15 min at RT. Next, cells were washed with a sequence of ethanol steps (twice with 50% ethanol for 20 min each, then once with 80% ethanol for 20 min) and then with Triton-PBS prior to mounting. The Thio S and α-synuclein staining has been described in detail (Stojkovska and Mazzulli, 2021). All images were obtained on a Leica confocal microscope, and image analysis was performed using ImageJ.

Measurement of Neuron viability through neurofilament quantification: For this assay, the same cultures used in the live cell activity were used from a 96 well plate. Following the live-cell lysosomal GCase activity assay, the cells were fixed in 4% paraformaldehyde in PBS for 15 minutes, and stained with an anti- neurofilament antibody overnight at 4°C (refer to (Mazzulli *et al.*, 2016a) for details). The next day, IRdye 800CW goat anti-mouse IgG secondary antibody and CellTag 700 stain were added to the wells and incubated for 1 hour, and the plate was scanned on a Li-Cor infrared imaging system.

Electron Microscopy (EM) analysis: Neurons were fixed in 2.5% glutaraldehyde (Electron Microscopy Sciences) in PBS for 30 minutes, and then washed six times with PBS for 5 minutes. Cells were post-fixed with 1% osmium tetroxide (OsO_4) (Electron Microscopy Sciences) in PBS for 1 hour, and then washed three times with H2O. Next, cells were dehydrated with ethanol (twice with 50% ethanol for 5 minutes, then twice with 70% ethanol for 10 minutes) and stained with 1% uranyl acetate (Electron Microscopy Sciences) in 70% ethanol for 45 minutes. Cells were further dehydrated with ethanol (once with 70% ethanol, then twice with 90% ethanol for 10 minutes, then three times with 100% ethanol for 10 minutes). To evaporate the ethanol, 100% ethanol was mixed at a 1:1 ratio with an LX112 resin mix containing LX112 (Ladd Research Industries), DDSA (Electron

Microscopy Sciences), and NMA (Electron Microscopy Sciences), and added to the cells for 1 hour with the lid off. Next, LX112 resin mix alone was added to the cells for 1 hour. Finally, cells were embedded by combining LX112 resin mix with DMP-30 (Electron Microscopy Sciences) and allowing the resin to solidify overnight at 60°C. Samples were then thin sectioned (~70nm width) on a UC7 ultramicrotome, as a service provided by the Northwestern University Center for Advanced Microscopy, and viewed on a FEI Tecnai Spirit G2 TEM. For each cell that was imaged via EM, all clearly defined ER regions were analyzed for both length and area using the 'Measure' function in ImageJ. The length and ER area (in micrometers) of each individual ER profile were plotted on a graph using GraphPad Prism. 3 to 9 cells per line were quantified and each data point on the scatter plot indicates a measured ER segment.

Proximity Ligation Assay (PLA): Inducible H4 cells overexpressing a-syn were treated with 1ug/ul DOX for 3 days to turn off α-syn expression. iPSC derived neurons were cultured to day 70 or 90 and separate batches were used for analysis. Cells were plated on coverglass were fixed with 4% paraformaldehyde for 20 minutes at RT. The cells were then washed three times with PBS, permeabilized with 0.3% Triton X-100 in PBS for 1 hour at 4°C, and then blocked with 2% BSA (Roche) and 5% NGS (Jackson Immuno Research) in Triton-PBS for 30 minutes at RT. Interaction between α-syn and ER chaperones was determined via the Duolink In Situ Red Starter Kit Mouse/Rabbit (Sigma). Cells were incubated with primary antibodies (anti-α-synuclein syn211, anti-α-synuclein C20, anti-CANX, anti-GRP94) overnight followed by a 1 hour, 37°C incubation with the PLA probes (secondary antibodies labeled with distinct oligonucleotides) provided in the kit. If the PLA probes are in proximity, the addition of ligase and DNA polymerase results in rolling circle amplification. For the ligation step, cells were washed twice with 1X wash buffer A (provided in the PLA kit) for 5 minutes each, and incubated with ligase (1:40 dilution) for 30 minutes at 37°C. For the amplification step, cells were washed twice with 1X wash buffer A for 2 minutes each, and incubated with polymerase diluted (1:80) in an amplification buffer containing fluorescently labeled complementary nucleotide probes for 100 minutes at 37°C. After the incubation, the cells were washed twice with 1X wash buffer B (provided in the PLA kit) for 10 minutes each followed by a quick wash with 0.01X wash buffer B. Finally, the cover glass was mounted onto microscope slides with DAPI mounting media. All images were obtained on a Leica confocal microscope (PLA excitation: 488nm). Counting of PLA particles was automated using ImageJ using the 'Measure' function. To determine the level of interaction, the number of PLA particles were normalized to the number of nuclei within an acquired field of view (n=5 FOV per condition), and expressed as a fold change to the +DOX condition.

Super-resolution structured illumination microscopy (SIM): iPSC neurons were plated on coverglass, fixed in 4% paraformaldehyde for 15 minutes, permeabilized with 0.1% Triton X-100 in PBS for 30 minutes, and blocked with 2% BSA and 5% NGS in Triton-PBS for 30 minutes. Primary antibodies (anti-α-synuclein syn211, anti-PDIA6) were added overnight, followed by incubation with secondary antibodies (Alexa Fluor 488 Goat anti-mouse IgG and Alexa Fluor 568 Goat anti-rabbit IgG) for 2 hours. The cells were then washed three times with Triton-PBS and mounted onto microscope slides with DAPI mounting media. Imaging was performed using an oil immersion 100X objective lens on a Nikon structured illumination microscope (N-SIM) at the Northwestern University Center for Advanced Microscopy. Images were captured and slices were reconstructed using the Nikon NIS Elements program.

Pharmacological treatment of cell cultures

ER stress induction of H4 cells or iPSC neurons: To induce ER stress and activate the UPR, H4 cells or iPSC neurons were treated with 30nM thapsigargin (Tg) (Sigma) or 50ng/ml brefeldin A (BFA) for 24 hours prior to harvesting, and analysis of mRNA and/or protein expression of known ER stress markers was performed.

Proteasomal inhibition of iPSC neurons: iPSC neurons were treated with 50 nM epoxomicin (Fisher) for 24 hours. Analysis of GCase levels following treatment was performed via western blot analysis. Successful proteasomal inhibition was confirmed by blotting for ubiquitin.

Treatment of H4 cells or iPSC neurons with ER proteostasis and trafficking enhancers: H4 cells or iPSC neurons were treated with vehicle or either 25μM diltiazem (DILT) (Sigma), 40μM dantrolene (DANT) (Sigma) or 1μm DHBP (Sigma), and media was changed every other day for the duration of the experiment. For the combination compound treatments, H4 cells or iPSC neurons were treated with vehicle, 25uM DILT, 5nM farnesyl transferase inhibitor (FTI) (gift of Peter T. Lansbury, Jr.), or FTI+DILT combination, and media was changed every other day for the duration of the experiment. For the combination of genetic manipulation and compound treatment (e.g. RyR3 KD + FTI, DILT + ykt6-CS), cells were infected and treatment was begun at the same time, with media change every other day for the duration of the experiment.

Lentiviral treatment of cell cultures

Lentiviral preparation and transduction of H4 cells and iPSC neurons: In combination with a packaging vector (psPAX2) and an envelope vector (VSV-G), lentiviral plasmids were used to create lentiviral particles by transfecting HEK293FT cells using X-tremeGENE transfection reagent (Roche). The lentiviral particles were collected and concentrated using Lenti-X concentrator (Clontech) and titered with a HIV1-p24 antigen ELISA kit (Zeptometrix). For RyR3 shRNA knock-down and ykt6-CS overexpression, H4 cells and iPSC neurons were infected at a multiplicity of infection (MOI) of 3–5 and were harvested 5 days or 2 weeks post-infection, respectively. For GBA1 L444P overexpression, neurons were infected at MOI of 1 and were harvested 2 weeks post-infection.

Ryanodine receptor RyR3 knockdown using shRNA constructs: MISSION shRNA sequences targeting human RyR3 were obtained from Sigma and tested for efficiency in HEK293T cells by quantitative RT-PCR analysis using RyR3 TaqMan probes. Clone ID #TRCN0000053349 was found to achieve the most efficient knock-down and was therefore used in subsequent experiments. This lentiviral plasmid was used to create lentiviral particles, as described under “Lentiviral preparation and transduction of H4 cells and iPSC neurons”.

Generation of the GBA1 L444P plasmid and transduction in iPSC-neurons: *GBA1* L444P was generated by site-directed mutagenesis (SDM) of the pER4-wild-type *GBA1* lentiviral plasmid. Mutagenesis primers (5'-GTGCCACTGCGTCCGGGTCGTTCTTCTGA-3' and 5'-TCAGAAGAACGACCCGGACGCAGTGGCAC-3') were created using the Agilent tool. SDM was performed using the materials and procedures from the QuikChange XL Site-Directed Mutagenesis Kit (Agilent). The L444P mutation was confirmed by sequencing. The pER4 *GBA1* L444P plasmid was then packaged into lentiviral particles, as described under "Lentiviral preparation and transduction of H4 cells and iPSC neurons".

QUANTIFICATION AND STATISTICAL ANALYSIS

Quantification methods of western blots and images have been described above. In each quantification, a single plot point indicates a separate biological replicate (individual culture well), taken from at least two distinct iPSC passages / differentiation batches. The value of n and what n represents is indicated in each figure legend. Analyzed data was plotted and tested for statistical significance using the GraphPad Prism software. Statistical significance between two samples was determined using a paired or unpaired t-test with Welch's correction. For more than two conditions, significance was determined using a one-way ANOVA with Tukey's post-hoc test. A p-value of <0.05 was considered to be significant (*$p < 0.05$, **$p < 0.01$, ***$p < 0.001$, ****$p < 0.0001$). For each quantification, the type of error bar used and statistical test is specified in the figure legends.

Supplementary Material

Refer to Web version on PubMed Central for supplementary material.

Acknowledgements:

This work was supported by the National Institute of Neurological Disorders and Stroke grant R01NS092823 (JRM), R21NS107770 (JRM), and the National Science Foundation fellowship (IS). We thank Sohee Jeon for technical support.

References

Abeliovich A, and Gitler AD (2016). Defects in trafficking bridge Parkinson's disease pathology and genetics. Nature 539, 207–216. 10.1038/nature20414. [PubMed: 27830778]

Abeliovich A, Schmitz Y, Farinas I, Choi-Lundberg D, Ho WH, Castillo PE, Shinsky N, Verdugo JM, Armanini M, Ryan A, et al. (2000). Mice lacking alpha-synuclein display functional deficits in the nigrostriatal dopamine system. Neuron 25, 239–252. 10.1016/s0896-6273(00)80886-7. [PubMed: 10707987]

Bellucci A, Navarria L, Zaltieri M, Falarti E, Bodei S, Sigala S, Battistin L, Spillantini M, Missale C, and Spano P (2011). Induction of the unfolded protein response by alpha-synuclein in experimental models of Parkinson's disease. J Neurochem 116, 588–605. 10.1111/j.1471-4159.2010.07143.x. [PubMed: 21166675]

Booth C, and Koch GL (1989). Perturbation of cellular calcium induces secretion of luminal ER proteins. Cell 59, 729–737. 10.1016/0092-8674(89)90019-6. [PubMed: 2510935]

Calfon M, Zeng H, Urano F, Till JH, Hubbard SR, Harding HP, Clark SG, and Ron D (2002). IRE1 couples endoplasmic reticulum load to secretory capacity by processing the XBP-1 mRNA. Nature 415, 92–96. 10.1038/415092a. [PubMed: 11780124]

Chang D, Nalls MA, Hallgrimsdottir IB, Hunkapiller J, van der Brug M, Cai F, International Parkinson's Disease Genomics, C., andMe Research, T., Kerchner GA, Ayalon G, et al. (2017). A meta-analysis of genome-wide association studies identifies 17 new Parkinson's disease risk loci. Nat Genet 49, 1511–1516. 10.1038/ng.3955. [PubMed: 28892059]

Chia R, Sabir MS, Bandres-Ciga S, Saez-Atienzar S, Reynolds RH, Gustavsson E, Walton RL, Ahmed S, Viollet C, Ding J, et al. (2021). Genome sequencing analysis identifies new loci associated with Lewy body dementia and provides insights into its genetic architecture. Nat Genet 10.1038/s41588-021-00785-3.

Chung CY, Khurana V, Auluck PK, Tardiff DF, Mazzulli JR, Soldner F, Baru V, Lou Y, Freyzon Y, Cho S, et al. (2013). Identification and rescue of α-synuclein toxicity in Parkinson patient-derived neurons. Science (New York, N.Y.) 342, 983–987. 10.1126/science.1245296.

Colla E, Coune P, Liu Y, Pletnikova O, Troncoso JC, Iwatsubo T, Schneider BL, and Lee MK (2012a). Endoplasmic reticulum stress is important for the manifestations of α-synucleinopathy in vivo. The Journal of neuroscience : the official journal of the Society for Neuroscience 32, 3306–3320. 10.1523/JNEUROSCI.5367-11.2012. [PubMed: 22399753]

Colla E, Jensen PH, Pletnikova O, Troncoso JC, Glabe C, and Lee MK (2012b). Accumulation of toxic alpha-synuclein oligomer within endoplasmic reticulum occurs in alpha-synucleinopathy in vivo. J Neurosci 32, 3301–3305. 10.1523/JNEUROSCI.5368-11.2012. [PubMed: 22399752]

Colla E, Panattoni G, Ricci A, Rizzi C, Rota L, Carucci N, Valvano V, Gobbo F, Capsoni S, Lee MK, and Cattaneo A (2018). Toxic properties of microsome-associated alpha-synuclein species in mouse primary neurons. Neurobiol Dis 111, 36–47. 10.1016/j.nbd.2017.12.004. [PubMed: 29246724]

Conway KA, Harper JD, and Lansbury PT (1998). Accelerated in vitro fibril formation by a mutant alpha-synuclein linked to early-onset Parkinson disease. Nat Med 4, 1318–1320. 10.1038/3311. [PubMed: 9809558]

Cooper AA, Gitler AD, Cashikar A, Haynes CM, Hill KJ, Bhullar B, Liu K, Xu K, Strathearn KE, Liu F, et al. (2006). Alpha-synuclein blocks ER-Golgi traffic and Rab1 rescues neuron loss in Parkinson's models. Science 313, 324–328. 10.1126/science.1129462. [PubMed: 16794039]

Credle JJ, Forcelli PA, Delannoy M, Oaks AW, Permaul E, Berry DL, Duka V, Wills J, and Sidhu A (2015). alpha-Synuclein-mediated inhibition of ATF6 processing into COPII vesicles disrupts UPR signaling in Parkinson's disease. Neurobiol Dis 76, 112–125. 10.1016/j.nbd.2015.02.005. [PubMed: 25725420]

Cuddy LK, and Mazzulli JR (2021). Analysis of lysosomal hydrolase trafficking and activity in human iPSC-derived neuronal models. STAR Protoc 2, 100340. 10.1016/j.xpro.2021.100340. [PubMed: 33659904]

Cuddy LK, Wani WY, Morella ML, Pitcairn C, Tsutsumi K, Fredriksen K, Justman CJ, Grammatopoulos TN, Belur NR, Zunke F, et al. (2019). Stress-Induced Cellular Clearance Is Mediated by the SNARE Protein ykt6 and Disrupted by alpha-Synuclein. Neuron 104, 869–884 e811. 10.1016/j.neuron.2019.09.001. [PubMed: 31648898]

Fernandes HJR, Hartfield EM, Christian HC, Emmanoulidou E, Zheng Y, Booth H, Bogetofte H, Lang C, Ryan BJ, Sardi SP, et al. (2016). ER Stress and Autophagic Perturbations Lead to Elevated Extracellular α-Synuclein in GBA-N370S Parkinson's iPSC-Derived Dopamine Neurons. Stem cell reports 6, 342–356. 10.1016/j.stemcr.2016.01.013. [PubMed: 26905200]

Fruen BR, Mickelson JR, and Louis CF (1997). Dantrolene inhibition of sarcoplasmic reticulum Ca2+ release by direct and specific action at skeletal muscle ryanodine receptors. J Biol Chem 272, 26965–26971. 10.1074/jbc.272.43.26965. [PubMed: 9341133]

Fuchs J, Nilsson C, Kachergus J, Munz M, Larsson EM, Schule B, Langston JW, Middleton FA, Ross OA, Hulihan M, et al. (2007). Phenotypic variation in a large Swedish pedigree due to SNCA duplication and triplication. Neurology 68, 916–922. 10.1212/01.wnl.0000254458.17630.c5. [PubMed: 17251522]

Fujiwara T, Oda K, Yokota S, Takatsuki A, and Ikehara Y (1988). Brefeldin A causes disassembly of the Golgi complex and accumulation of secretory proteins in the endoplasmic reticulum. J Biol Chem 263, 18545–18552. [PubMed: 3192548]

Garcia-Sanz P, Orgaz L, Bueno-Gil G, Espadas I, Rodriguez-Traver E, Kulisevsky J, Gutierrez A, Davila JC, Gonzalez-Polo RA, Fuentes JM, et al. (2017). N370S-GBA1 mutation causes lysosomal cholesterol accumulation in Parkinson's disease. Mov Disord 32, 1409–1422. 10.1002/mds.27119. [PubMed: 28779532]

Gitler AD, Bevis BJ, Shorter J, Strathearn KE, Hamamichi S, Su LJ, Caldwell KA, Caldwell GA, Rochet JC, McCaffery JM, et al. (2008). The Parkinson's disease protein alpha-synuclein disrupts cellular Rab homeostasis. Proc Natl Acad Sci U S A 105, 145–150. 10.1073/pnas.0710685105. [PubMed: 18162536]

Gorbatyuk MS, Shabashvili A, Chen W, Meyers C, Sullivan LF, Salganik M, Lin JH, Lewin AS, Muzyczka N, and Gorbatyuk OS (2012). Glucose regulated protein 78 diminishes alpha-synuclein neurotoxicity in a rat model of Parkinson disease. Mol Ther 20, 1327–1337. 10.1038/mt.2012.28. [PubMed: 22434142]

Gosavi N, Lee HJ, Lee JS, Patel S, and Lee SJ (2002). Golgi fragmentation occurs in the cells with prefibrillar alpha-synuclein aggregates and precedes the formation of fibrillar inclusion. J Biol Chem 277, 48984–48992. 10.1074/jbc.M208194200. [PubMed: 12351643]

Grandjean JMD, Madhavan A, Cech L, Seguinot BO, Paxman RJ, Smith E, Scampavia L, Powers ET, Cooley CB, Plate L, et al. (2020). Pharmacologic IRE1/XBP1s activation confers targeted ER proteostasis reprogramming. Nat Chem Biol 16, 1052–1061. 10.1038/s41589-020-0584-z. [PubMed: 32690944]

Guardia-Laguarta C, Area-Gomez E, Rub C, Liu Y, Magrane J, Becker D, Voos W, Schon EA, and Przedborski S (2014). alpha-Synuclein is localized to mitochondria-associated ER membranes. J Neurosci 34, 249–259. 10.1523/JNEUROSCI.2507-13.2014. [PubMed: 24381286]

Harding HP, Zhang Y, and Ron D (1999). Protein translation and folding are coupled by an endoplasmic-reticulum-resident kinase. Nature 397, 271–274. 10.1038/16729. [PubMed: 9930704]

Helms JB, and Rothman JE (1992). Inhibition by brefeldin A of a Golgi membrane enzyme that catalyses exchange of guanine nucleotide bound to ARF. Nature 360, 352–354. 10.1038/360352a0. [PubMed: 1448152]

Heman-Ackah SM, Manzano R, Hoozemans JJM, Scheper W, Flynn R, Haerty W, Cowley SA, Bassett AR, and Wood MJA (2017). Alpha-synuclein induces the unfolded protein response in Parkinson's disease SNCA triplication iPSC-derived neurons. Hum Mol Genet 26, 4441–4450. 10.1093/hmg/ddx331. [PubMed: 28973645]

Hernandez I, Luna G, Rauch JN, Reis SA, Giroux M, Karch CM, Boctor D, Sibih YE, Storm NJ, Diaz A, et al. (2019). A farnesyltransferase inhibitor activates lysosomes and reduces tau pathology in mice with tauopathy. Sci Transl Med 11. 10.1126/scitranslmed.aat3005.

Hoozemans JJ, van Haastert ES, Eikelenboom P, de Vos RA, Rozemuller JM, and Scheper W (2007). Activation of the unfolded protein response in Parkinson's disease. Biochem Biophys Res Commun 354, 707–711. 10.1016/j.bbrc.2007.01.043. [PubMed: 17254549]

Hunn BH, Cragg SJ, Bolam JP, Spillantini MG, and Wade-Martins R (2015). Impaired intracellular trafficking defines early Parkinson's disease. Trends Neurosci 38, 178–188. 10.1016/j.tins.2014.12.009. [PubMed: 25639775]

Kang JJ, Hsu KS, and Lin-Shiau SY (1994). Effects of bipyridylium compounds on calcium release from triadic vesicles isolated from rabbit skeletal muscle. Br J Pharmacol 112, 1216–1222. 10.1111/j.1476-5381.1994.tb13213.x. [PubMed: 7952884]

Klein AD, and Mazzulli JR (2018). Is Parkinson's disease a lysosomal disorder? Brain 141, 2255–2262. 10.1093/brain/awy147. [PubMed: 29860491]

Kozutsumi Y, Segal M, Normington K, Gething MJ, and Sambrook J (1988). The presence of malfolded proteins in the endoplasmic reticulum signals the induction of glucose-regulated proteins. Nature 332, 462–464. 10.1038/332462a0. [PubMed: 3352747]

Kriks S, Shim JW, Piao J, Ganat YM, Wakeman DR, Xie Z, Carrillo-Reid L, Auyeung G, Antonacci C, Buch A, et al. (2011). Dopamine neurons derived from human ES cells efficiently engraft in animal models of Parkinson's disease. Nature 480, 547–551. 10.1038/nature10648. [PubMed: 22056989]

Lee AH, Iwakoshi NN, and Glimcher LH (2003). XBP-1 regulates a subset of endoplasmic reticulum resident chaperone genes in the unfolded protein response. Mol Cell Biol 23, 7448–7459. 10.1128/mcb.23.21.7448-7459.2003. [PubMed: 14559994]

Marquardt T, and Helenius A (1992). Misfolding and aggregation of newly synthesized proteins in the endoplasmic reticulum. J Cell Biol 117, 505–513. 10.1083/jcb.117.3.505. [PubMed: 1315315]

Martin I, Kim JW, Dawson VL, and Dawson TM (2014). LRRK2 pathobiology in Parkinson's disease. J Neurochem 131, 554–565. 10.1111/jnc.12949. [PubMed: 25251388]

Masliah E, Rockenstein E, Veinbergs I, Mallory M, Hashimoto M, Takeda A, Sagara Y, Sisk A, and Mucke L (2000). Dopaminergic loss and inclusion body formation in alpha-synuclein mice: implications for neurodegenerative disorders. Science 287, 1265–1269. 10.1126/science.287.5456.1265. [PubMed: 10678833]

Mazzulli JR, Xu YH, Sun Y, Knight AL, McLean PJ, Caldwell GA, Sidransky E, Grabowski GA, and Krainc D (2011). Gaucher disease glucocerebrosidase and alpha-synuclein form a bidirectional pathogenic loop in synucleinopathies. Cell 146, 37–52. 10.1016/j.cell.2011.06.001. [PubMed: 21700325]

Mazzulli JR, Zunke F, Isacson O, Studer L, and Krainc D (2016a). alpha-Synucleininduced lysosomal dysfunction occurs through disruptions in protein trafficking in human midbrain synucleinopathy models. Proc Natl Acad Sci U S A 113, 1931–1936. 10.1073/pnas.1520335113. [PubMed: 26839413]

Mazzulli JR, Zunke F, Isacson O, Studer L, and Krainc D (2016b). alpha-Synuclein-induced lysosomal dysfunction occurs through disruptions in protein trafficking in human midbrain synucleinopathy models. Proc Natl Acad Sci U S A 113, 1931–1936. 10.1073/pnas.1520335113. [PubMed: 26839413]

Melnick J, Dul JL, and Argon Y (1994). Sequential interaction of the chaperones BiP and GRP94 with immunoglobulin chains in the endoplasmic reticulum. Nature 370, 373–375. 10.1038/370373a0. [PubMed: 7913987]

Mu TW, Ong DS, Wang YJ, Balch WE, Yates JR 3rd, Segatori L, and Kelly JW (2008). Chemical and biological approaches synergize to ameliorate protein-folding diseases. Cell 134, 769–781. 10.1016/j.cell.2008.06.037. [PubMed: 18775310]

Nalls MA, Pankratz N, Lill CM, Do CB, Hernandez DG, Saad M, DeStefano AL, Kara E, Bras J, Sharma M, et al. (2014). Large-scale meta-analysis of genome-wide association data identifies six new risk loci for Parkinson's disease. Nat Genet 46, 989–993. 10.1038/ng.3043. [PubMed: 25064009]

Ong DST, Mu T-W, Palmer AE, and Kelly JW (2010). Endoplasmic reticulum Ca2+ increases enhance mutant glucocerebrosidase proteostasis. Nature chemical biology 6, 424–432. 10.1038/nchembio.368. [PubMed: 20453863]

Ou WJ, Cameron PH, Thomas DY, and Bergeron JJ (1993). Association of folding intermediates of glycoproteins with calnexin during protein maturation. Nature 364, 771–776. 10.1038/364771a0. [PubMed: 8102790]

Paillusson S, Gomez-Suaga P, Stoica R, Little D, Gissen P, Devine MJ, Noble W, Hanger DP, and Miller CCJ (2017). alpha-Synuclein binds to the ER-mitochondria tethering protein VAPB to disrupt Ca(2+) homeostasis and mitochondrial ATP production. Acta Neuropathol 134, 129–149. 10.1007/s00401-017-1704-z. [PubMed: 28337542]

Price BD, Mannheim-Rodman LA, and Calderwood SK (1992). Brefeldin A, thapsigargin, and AIF4- stimulate the accumulation of GRP78 mRNA in a cycloheximide dependent manner, whilst induction by hypoxia is independent of protein synthesis. J Cell Physiol 152, 545–552. 10.1002/jcp.1041520314. [PubMed: 1506413]

Proia RL, and Neufeld EF (1982). Synthesis of beta-hexosaminidase in cell-free translation and in intact fibroblasts: an insoluble precursor alpha chain in a rare form of Tay-Sachs disease. Proc Natl Acad Sci U S A 79, 6360–6364. 10.1073/pnas.79.20.6360. [PubMed: 6959123]

Rajagopalan S, Xu Y, and Brenner MB (1994). Retention of unassembled components of integral membrane proteins by calnexin. Science 263, 387–390. 10.1126/science.8278814. [PubMed: 8278814]

Reczek D, Schwake M, Schroder J, Hughes H, Blanz J, Jin XY, Brondyk W, Van Patten S, Edmunds T, and Saftig P (2007). LIMP-2 is a receptor for lysosomal mannose-6-phosphate-independent targeting of beta-Glucocerebrosidase. Cell 131, 770–783. 10.1016/j.cell.2007.10.018. [PubMed: 18022370]

Robak LA, Jansen IE, van Rooij J, Uitterlinden AG, Kraaij R, Jankovic J, International Parkinson's Disease Genomics, C., Heutink P, and Shulman JM (2017). Excessive burden of lysosomal storage disorder gene variants in Parkinson's disease. Brain 140, 3191–3203. 10.1093/brain/awx285. [PubMed: 29140481]

Ron I, and Horowitz M (2005). ER retention and degradation as the molecular basis underlying Gaucher disease heterogeneity. Hum Mol Genet 14, 2387–2398. 10.1093/hmg/ddi240. [PubMed: 16000318]

Roshan Lal T, and Sidransky E (2017). The Spectrum of Neurological Manifestations Associated with Gaucher Disease. Diseases 5. 10.3390/diseases5010010.

Rothaug M, Zunke F, Mazzulli JR, Schweizer M, Altmeppen H, Lullmann-Rauch R, Kallemeijn WW, Gaspar P, Aerts JM, Glatzel M, et al. (2014). LIMP-2 expression is critical for beta-glucocerebrosidase activity and alpha-synuclein clearance. Proc Natl Acad Sci U S A 111, 15573–15578. 10.1073/pnas.1405700111. [PubMed: 25316793]

Schuck S, Prinz WA, Thorn KS, Voss C, and Walter P (2009). Membrane expansion alleviates endoplasmic reticulum stress independently of the unfolded protein response. J Cell Biol 187, 525–536. 10.1083/jcb.200907074. [PubMed: 19948500]

Sidransky E, Nalls MA, Aasly JO, Aharon-Peretz J, Annesi G, Barbosa ER, Bar-Shira A, Berg D, Bras J, Brice A, et al. (2009). Multicenter analysis of glucocerebrosidase mutations in Parkinson's disease. N Engl J Med 361, 1651–1661. 10.1056/NEJMoa0901281. [PubMed: 19846850]

Simon-Sanchez J, Schulte C, Bras JM, Sharma M, Gibbs JR, Berg D, Paisan-Ruiz C, Lichtner P, Scholz SW, Hernandez DG, et al. (2009). Genome-wide association study reveals genetic risk underlying Parkinson's disease. Nat Genet 41, 1308–1312. 10.1038/ng.487. [PubMed: 19915575]

Singh PK, and Muqit MMK (2020). Parkinson's: A Disease of Aberrant Vesicle Trafficking. Annu Rev Cell Dev Biol 36, 237–264. 10.1146/annurev-cellbio-100818-125512. [PubMed: 32749865]

Singleton AB, Farrer M, Johnson J, Singleton A, Hague S, Kachergus J, Hulihan M, Peuralinna T, Dutra A, Nussbaum R, et al. (2003). alpha-Synuclein locus triplication causes Parkinson's disease. Science 302, 841. 10.1126/science.1090278. [PubMed: 14593171]

Smith MH, Ploegh HL, and Weissman JS (2011). Road to ruin: targeting proteins for degradation in the endoplasmic reticulum. Science 334, 1086–1090. 10.1126/science.1209235. [PubMed: 22116878]

Soldner F, Laganiere J, Cheng AW, Hockemeyer D, Gao Q, Alagappan R, Khurana V, Golbe LI, Myers RH, Lindquist S, et al. (2011). Generation of isogenic pluripotent stem cells differing exclusively at two early onset Parkinson point mutations. Cell 146, 318–331. 10.1016/j.cell.2011.06.019. [PubMed: 21757228]

Spillantini MG, Schmidt ML, Lee VM, Trojanowski JQ, Jakes R, and Goedert M (1997). Alpha-synuclein in Lewy bodies. Nature 388, 839–840. 10.1038/42166. [PubMed: 9278044]

Stojkovska I, and Mazzulli JR (2021). Detection of pathological alpha-synuclein aggregates in human iPSC-derived neurons and tissue. STAR Protoc 2, 100372. 10.1016/j.xpro.2021.100372. [PubMed: 33733241]

Sun Y, Liou B, Quinn B, Ran H, Xu YH, and Grabowski GA (2009). In vivo and ex vivo evaluation of L-type calcium channel blockers on acid beta-glucosidase in Gaucher disease mouse models. PLoS One 4, e7320. 10.1371/journal.pone.0007320. [PubMed: 19809509]

Tan YL, Genereux JC, Pankow S, Aerts JM, Yates JR 3rd, and Kelly JW (2014). ERdj3 is an endoplasmic reticulum degradation factor for mutant glucocerebrosidase variants linked to Gaucher's disease. Chem Biol 21, 967–976. 10.1016/j.chembiol.2014.06.008. [PubMed: 25126989]

Thayanidhi N, Helm JR, Nycz DC, Bentley M, Liang Y, and Hay JC (2010). Alpha-synuclein delays endoplasmic reticulum (ER)-to-Golgi transport in mammalian cells by antagonizing ER/Golgi SNAREs. Mol Biol Cell 21, 1850–1863. 10.1091/mbc.E09-09-0801. [PubMed: 20392839]

Vidal RL, Sepulveda D, Troncoso-Escudero P, Garcia-Huerta P, Gonzalez C, Plate L, Jerez C, Canovas J, Rivera CA, Castillo V, et al. (2021). Enforced dimerization between XBP1s and ATF6f enhances the protective effects of the UPR in models of neurodegeneration. Mol Ther. 10.1016/j.ymthe.2021.01.033.

Walter P, and Ron D (2011). The unfolded protein response: from stress pathway to homeostatic regulation. Science 334, 1081–1086. 10.1126/science.1209038. [PubMed: 22116877]

Wang F, Agnello G, Sotolongo N, and Segatori L (2011). Ca2+ homeostasis modulation enhances the amenability of L444P glucosylcerebrosidase to proteostasis regulation in patient-derived fibroblasts. ACS Chem Biol 6, 158–168. 10.1021/cb100321m. [PubMed: 21043486]

Wang M, and Kaufman RJ (2016). Protein misfolding in the endoplasmic reticulum as a conduit to human disease. Nature 529, 326–335. 10.1038/nature17041. [PubMed: 26791723]

Wiesmann UN, Lightbody J, Vassella F, and Herschkowitz NN (1971). Multiple lysosomal enzyme deficiency due to enzyme leakage? N Engl J Med 284, 109–110. 10.1056/NEJM197101142840220.

Yoshida H, Matsui T, Yamamoto A, Okada T, and Mori K (2001). XBP1 mRNA is induced by ATF6 and spliced by IRE1 in response to ER stress to produce a highly active transcription factor. Cell 107, 881–891. 10.1016/s0092-8674(01)00611-0. [PubMed: 11779464]

Zunke F, and Mazzulli JR (2019). Modeling neuronopathic storage diseases with patient-derived culture systems. Neurobiol Dis 127, 147–162. 10.1016/j.nbd.2019.01.018. [PubMed: 30790616]

Zunke F, Moise AC, Belur NR, Gelyana E, Stojkovska I, Dzaferbegovic H, Toker NJ, Jeon S, Fredriksen K, and Mazzulli JR (2018). Reversible Conformational Conversion of alpha-Synuclein into Toxic Assemblies by Glucosylceramide. Neuron 97, 92–107 e110. 10.1016/j.neuron.2017.12.012. [PubMed: 29290548]

Highlights

- α-Syn accumulation induces ER fragmentation in patient-derived midbrain neurons
- α-Syn perturbs the ability to recognize and respond to misfolded proteins in the ER
- Parkinson neurons develop pathogenic aggregates of immature lysosomal GCase
- GCase solubility/function is rescued by enhancing folding in the ER and trafficking

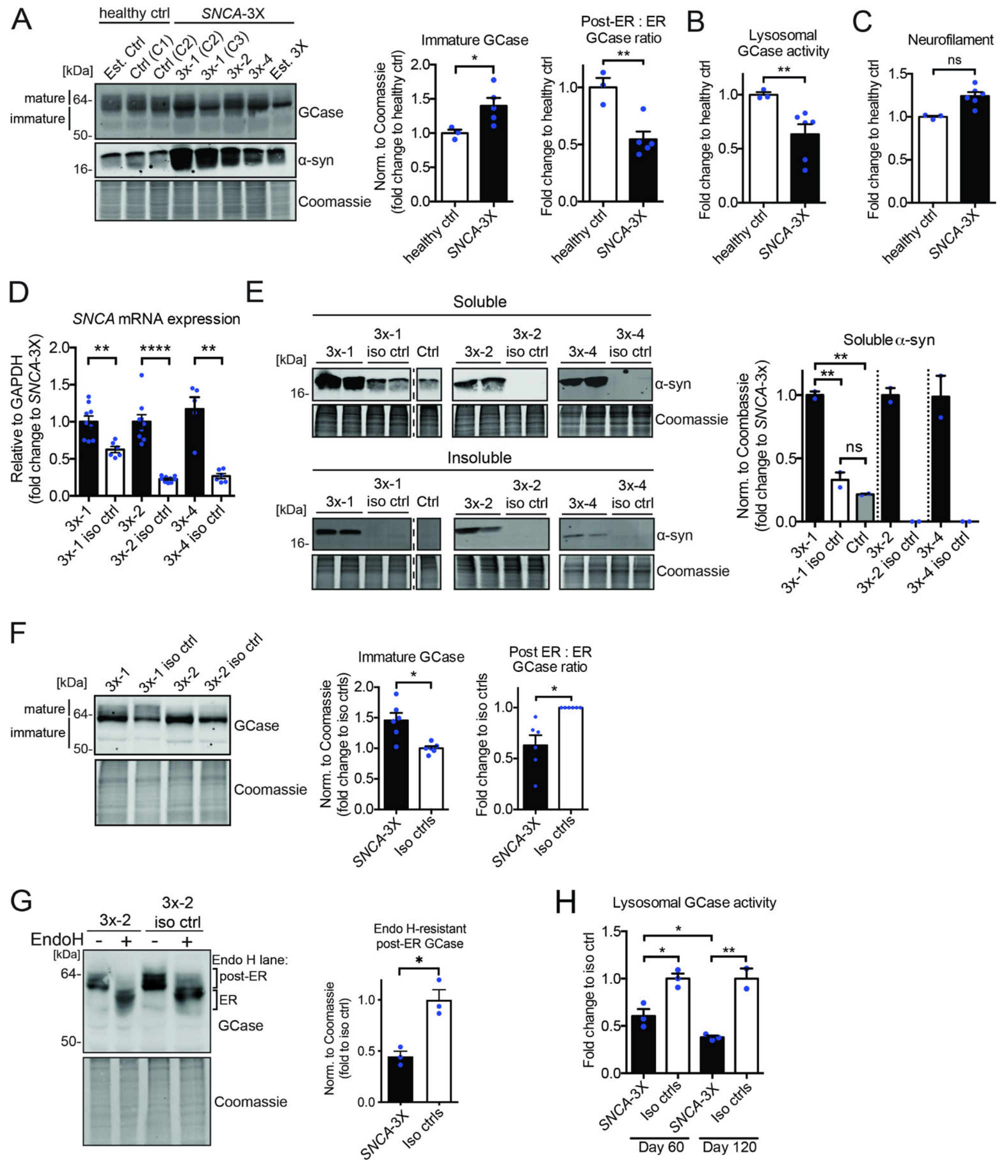

Figure 1. Defects in GCase maturation and lysosomal function in novel *SNCA*-3X midbrain DA lines.

A) Western blot of GCase and a-syn in day 90 neurons. Quantification is on the right. Coomassie was used as a loading control. **B)** Live-cell lysosomal GCase activity. **C)** Neurofilament quantification of day 90 neurons. **D)** Quantitative RT-PCR analysis of *SNCA* mRNA expression of day 90 DA neurons from 3X and isogenic controls (iso ctrl). **E)** Western blot of soluble and insoluble α-syn (antibody C20). Quantification is shown on the right as a fold change to each parental *SNCA*-3X line. Irrelevant lanes were cropped, indicated by a dashed line. **F)** Western blot of GCase maturation in day 90 *SNCA*-3X and isogenic controls. Right, quantification from each line 3X-1, 2, 4) and isogenic controls (n=2 from each line). **G)** GCase western blot of endoglycosidase H (Endo H) digested lysates of day 120 3X-2 neurons. Right, quantification of endo H-resistant GCase. **H)** Live-cell lysosomal GCase activity of 3X-1 and isogenic controls. For all quantifications, values are mean ± SEM, *p < 0.05; **p < 0.01; ****p < 0.0001; ns = not significant, using student's unpaired t-test.

Author Manuscript
Author Manuscript
Author Manuscript

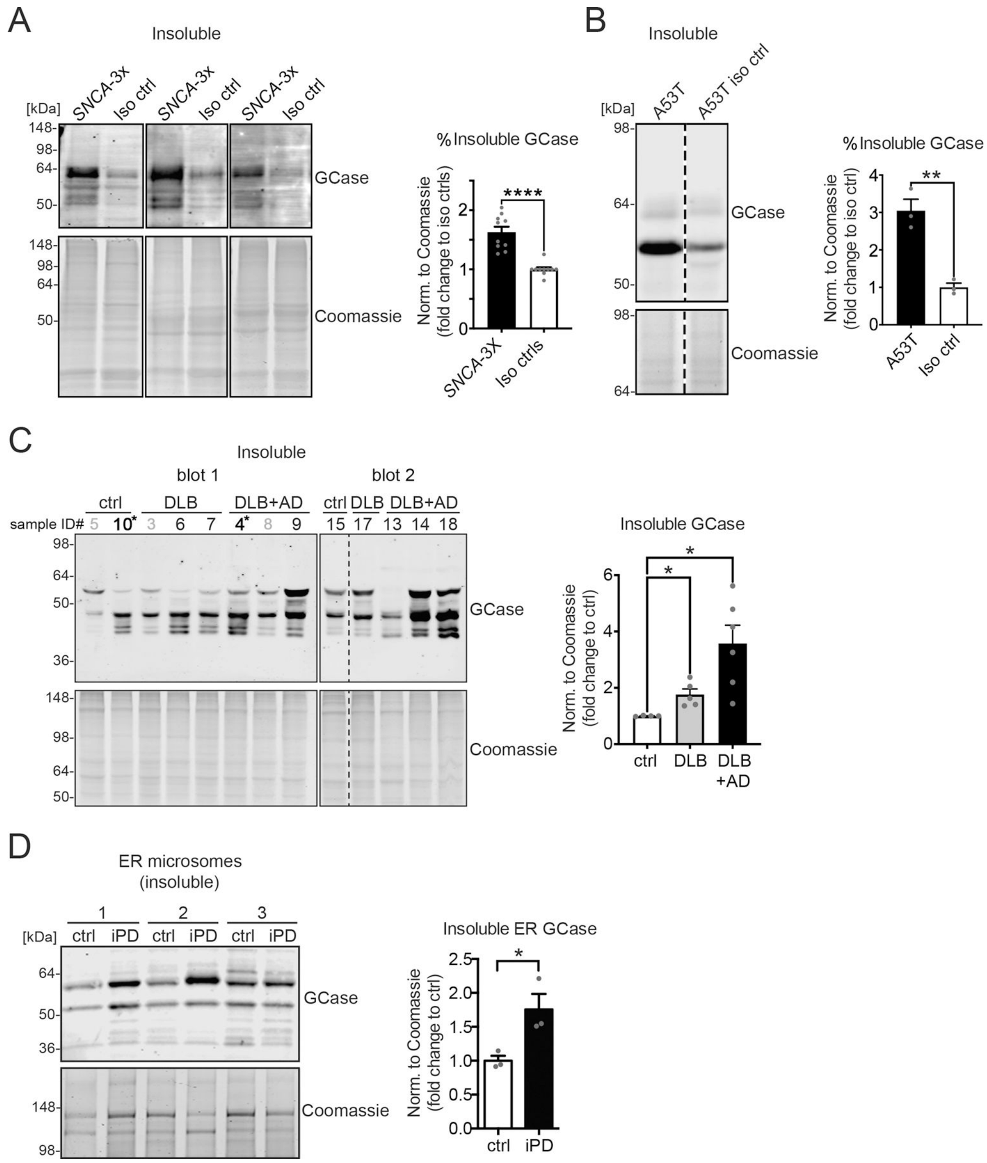

Figure 2. Accumulation of insoluble immature GCase in SNCA-3x midbrain DA neurons and synucleinopathy brains

(A) Western blot of Triton X-100 insoluble fractions from day 90 *SNCA*-3X and isogenic control DA neurons. 3x-4 is shown as a representative example. Right, quantification of % insoluble GCase from combined lines 3x-1, 3x-2, and 3x-4 (n = 3–4 from each), expressed as fold change. (B) Insoluble GCase from a PD line expressing A53T a-syn and its isogenic control at day 90 was analyzed as in (A). (C) GCase western blot of 1% sarkosyl-insoluble extracts from the frontal cortex of controls and synucleinopathy brains (DLB, dementia with Lewy bodies; DLB + AD, DLB with Alzheimer's disease [AD] pathology). Right: quantification of insoluble GCase/Coomassie, grouped by similar post-mortem intervals (PMI) (gray, PMI = <10 h; black, PMI < 20 h; asterisk, PMI < 30 h). See Table S1 for details. (D) Quantification of insoluble GCase from ER microsome fractions extracted from the cingulate cortex of controls and idiopathic PD brains. See Table S2 for details. For all quantifications, values are the mean ± SEM, *p < 0.05; **p < 0.01, using Student's unpaired t test (A, B, and D) or ANOVA with Dunnett's T3 test (C). In (B) and (C), irrelevant lanes were cropped, indicated by a dashed line.

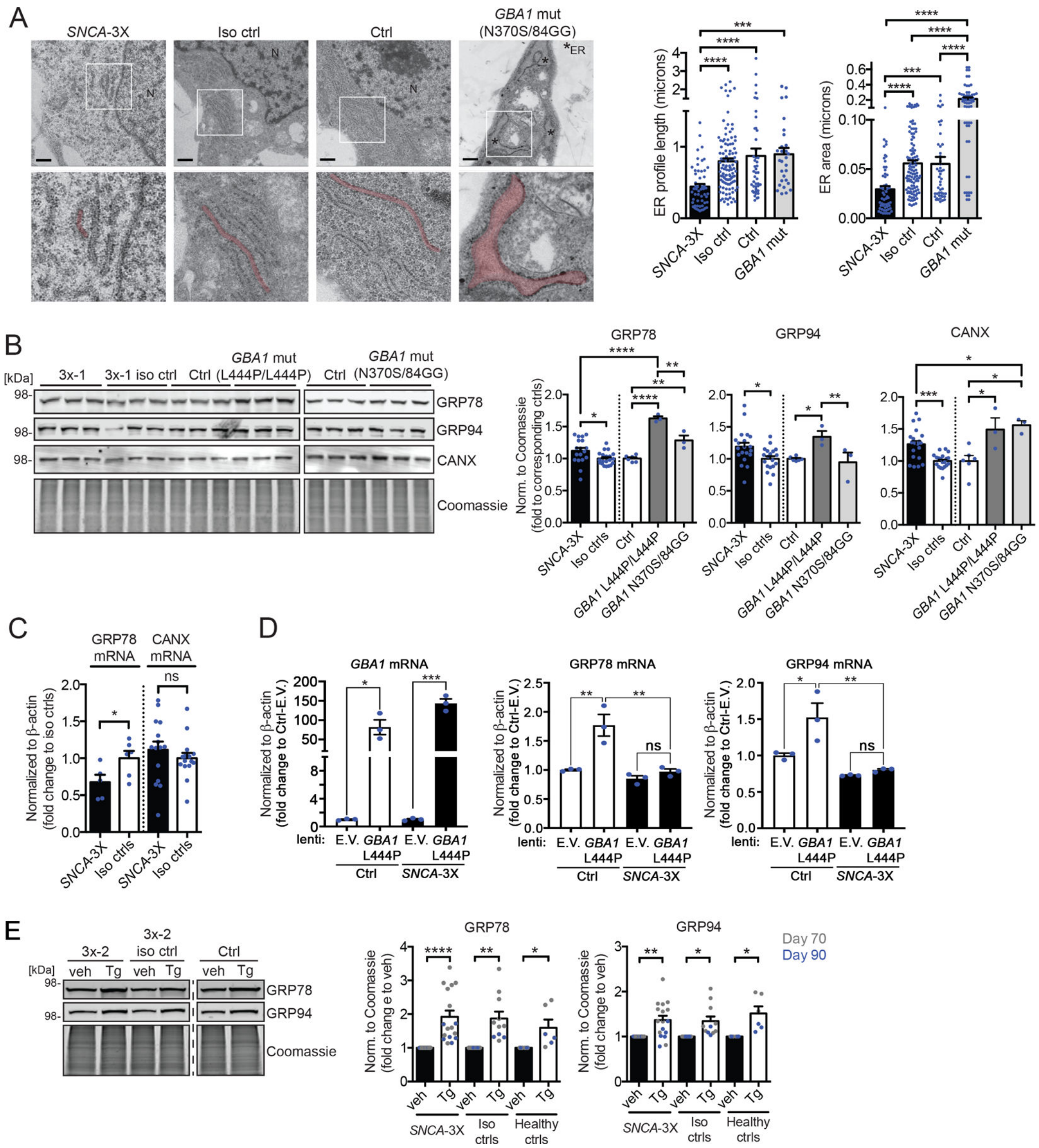

Figure 3. Characterization of ER morphology and ER stress response in *SNCA*-3X midbrain DA neurons.

A) Electron microscopy analysis showing representative ER ultrastructure of day 65 *SNCA*-3X (3x-2), mutant *GBA1* (N370S / 84GG), and control DA neurons. Examples of ER segments are highlighted in red. The white boxes show zoomed-in regions of the images below. N=nucleus, * = ER. Scale bar, 500 nm. Right, quantifications of ER length and area (n=3–9 cells per line; each data point on the scatter plot indicates a measured ER segment). **B)** Western blot of ER chaperones in day 90 *SNCA*-3X, mutant *GBA1* (N370S / 84GG and L444P / L444P), and control DA neurons (n=2–5 for each line). Right, quantification of *SNCA*-3X lines (3x-1, 3x-2, 3x-4) and mutant *GBA1* lines. **C)** RT-PCR analysis of GRP78 and CANX mRNA. **D)** RT-PCR analysis of day 90 control and *SNCA*-3X (3x-2) neurons infected to overexpress L444P GBA1 (MOI=1; dpi 14 days), to quantify mRNA of *GBA1*, GRP78, and GRP94. **E)** Western blot of 3X and control neurons after treatment with vehicle (veh) or 30 nM thapsigargin (Tg) for 24 hours Right, Quantification from 3x-1, 3x-2, 3x-4 and controls. Irrelevant lanes were cropped, indicated by a dashed line. For all quantifications, values are mean ± SEM, *$p < 0.05$; **$p < 0.01$; ***$p < 0.001$; ****$p < 0.0001$; ns = not significant, using student's unpaired (panels B,C), paired t-test (panel E), or ANOVA with Tukey's post-hoc test (panels A,B,D).

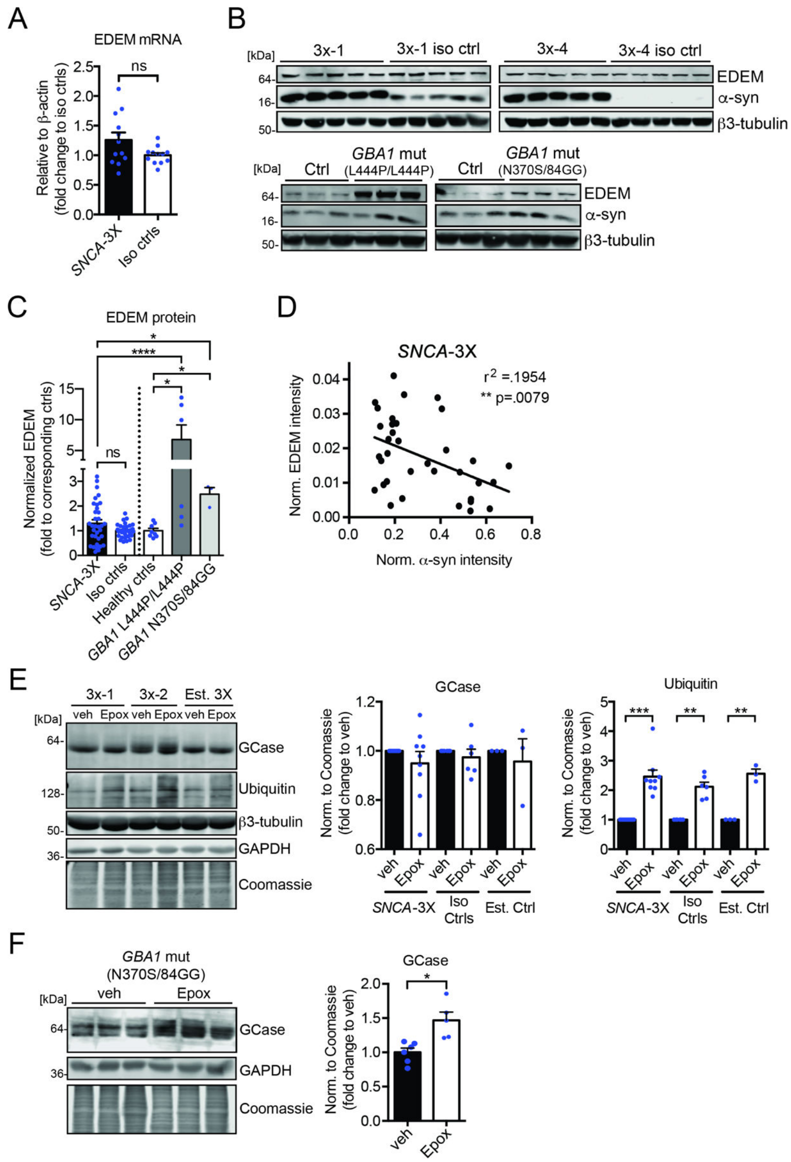

Figure 4. Analysis of EDEM expression and ERAD in *SNCA*-3X midbrain DA neurons.

A) RT-PCR analysis of EDEM1 mRNA in day 90 *SNCA*-3X and isogenic controls (combined 3X-1, 2, 4 and the corresponding isogenic controls, n=4 per line). **B)** Representative western blot of EDEM1 in day 90 *SNCA*-3X and *GBA1* mutant DA neurons. **C)** Western blot quantification of EDEM1 protein in *SNCA*-3X (combined 3X-1, 2, 4) and *GBA1* mutant DA neurons. **(D)** Correlation analysis of EDEM1 and α-syn protein obtained from western blots from different biological replicates of *SNCA*-3X patient DA neurons. **E)** Western blot of day 90 DA neurons treated with 50nM epoxomicin (Epox) for 24 hrs. Right, quantification of GCase and ubiquitin (combined from 3X-1, 2 and isogenic controls; n=3 per line). Coomassie, β3 tubulin and GAPDH were used as loading controls. **F)** GCase western blot of Epox treated *GBA1* mutant DA neurons. Quantification is shown on the right. For all quantifications, values are mean ± SEM, *p < 0.05; **p < 0.01; ***p < 0.001;

****p < 0.0001; ns = not significant, using student's unpaired (panels A,C,E,F) or paired t-test (E) or ANOVA with Tukey's post-hoc test (C).

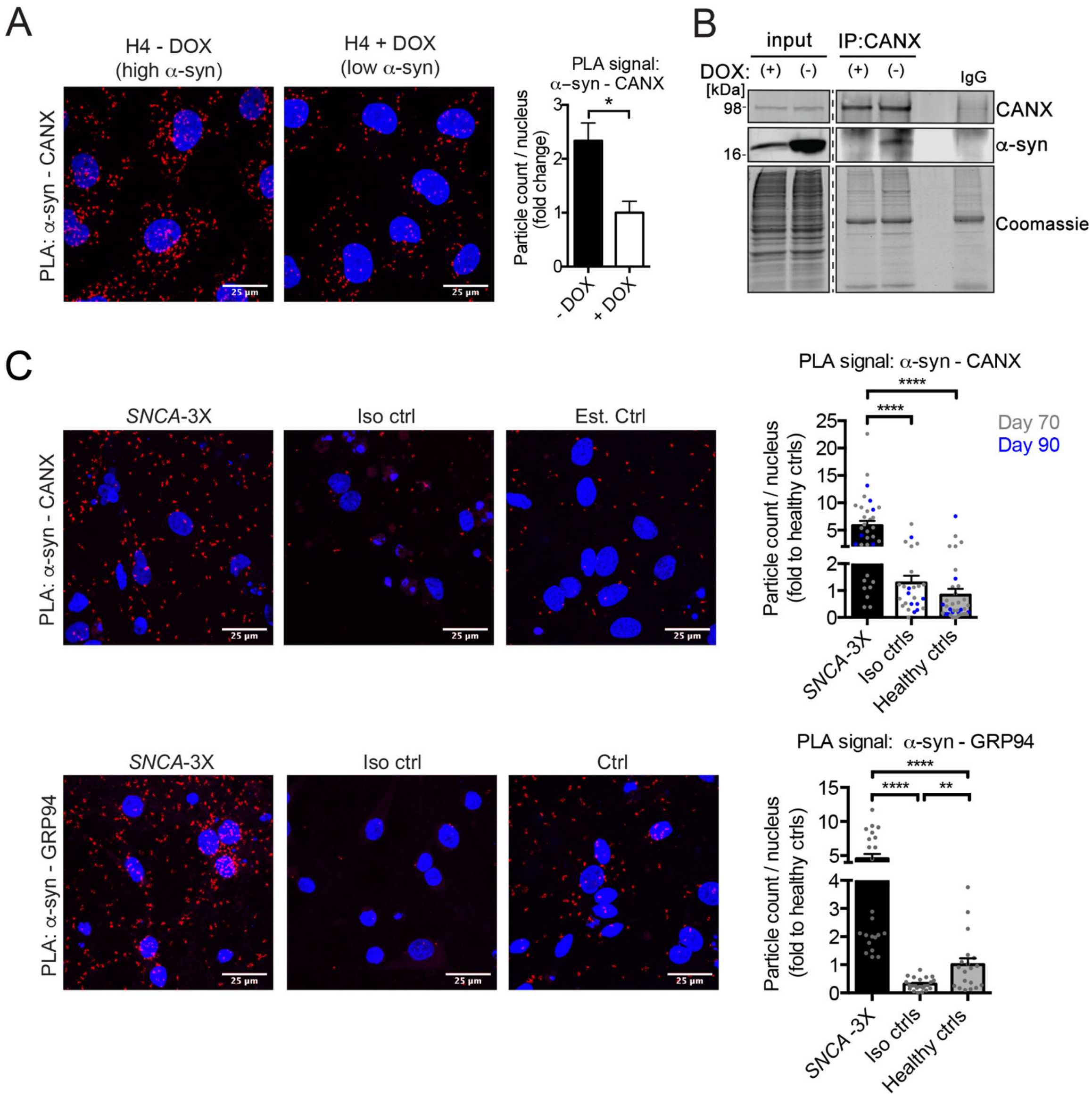

Figure 5. Increased association of a-syn with ER chaperones.

A) Proximity ligation assay (PLA) of inducible H4 cells overexpressing wild-type α-syn using anti-CANX and anti-a-syn antibodies (colocalization is indicated by a red dot). Nuclei are stained with DAPI (blue). Right, quantification of PLA signal. Scale bar, 25um. **B)** H4 lysates were immunoprecipitated with anti-CANX antibodies followed by western blot for a-syn and CANX. Irrelevant lanes were cropped, indicated by a dashed line. **C)** PLA was done in day 70 DA neurons (shown, 3X-2) to assess CANX **(top)** and GRP94 **(bottom)** associations with a-syn. Isogenic control for 3X-2 was used to assess background signal. Right, Quantification of PLA signal was quantified as in A using n=3–4 biological replicates per 3X line. Scale bar, 25um. For all quantifications, values are mean ± SEM, $*p < 0.05$; $**p < 0.01$; $****p < 0.0001$, using student's unpaired t-test (panel A) or ANOVA with Tukey's post-hoc test (panel B).

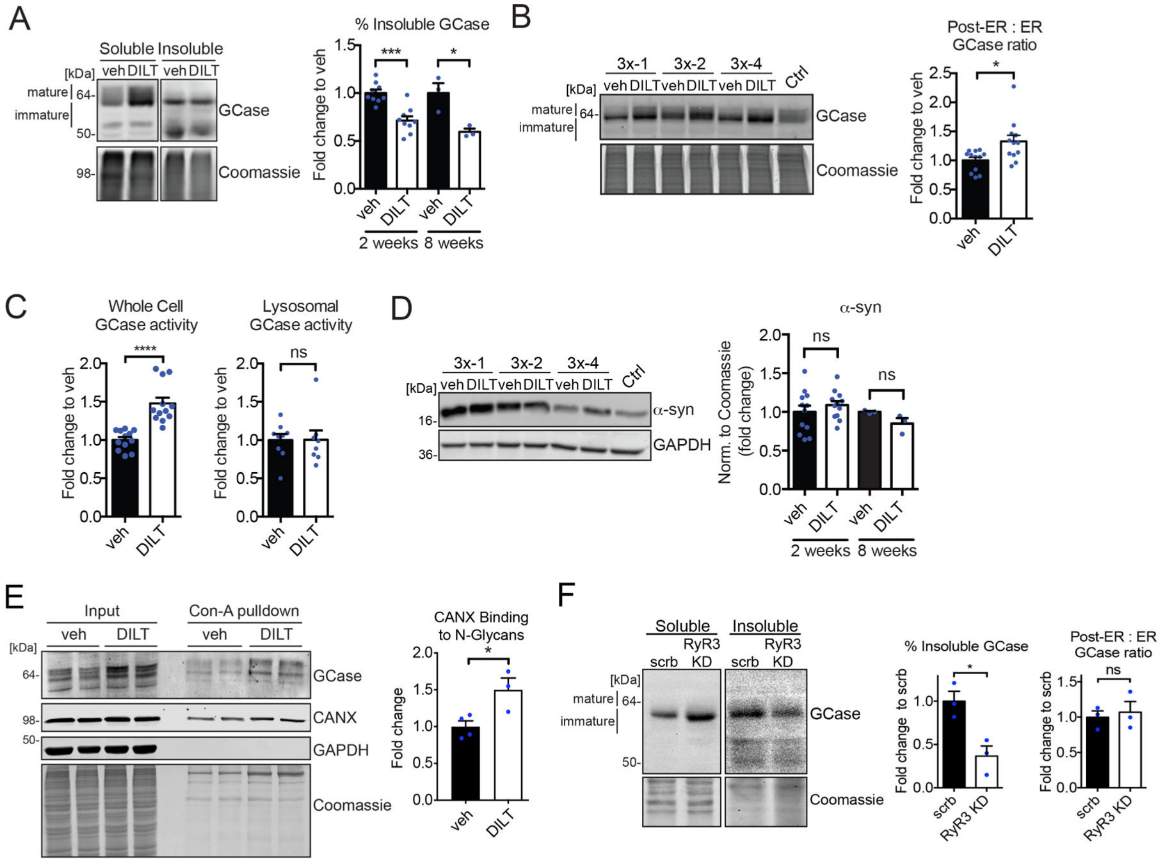

Figure 6. Enhancement of ER proteostasis improves GCase solubility and function in *SNCA*-3X DA neurons but fails to reduce a-synuclein.

A) GCase solubility analysis by western blot of day 90 *SNCA*-3X DA neurons treated with vehicle (veh) or 25μM diltiazem (DILT) for 2 or 8 weeks. Representative blot image is from 8 week 3x-1 DA neurons. Quantification from combined 3X lines is shown on the right. **B)** Western blot of GCase of day 90 *SNCA*-3X DA neurons treated with DILT for 2 weeks. Right, quantification of GCase maturation from lines 3x-1, 2, and 4 (n=3 per line). **C)** Left, whole cell GCase activity of *SNCA*-3X lysates from panel B. Right, live-cell lysosomal GCase activity in day 90 *SNCA*-3X DA neurons (2 weeks DILT). **D)** Western blot of α-syn levels (the same blot from panel B was reprobed for α-syn and quantified on the right). GAPDH is a loading control. **E)** CANX activity was assessed in H4 α-syn cells treated with DILT (5 days) by precipitation of N-glycosylated proteins with concanavalin A (Con-A) followed by CANX western blot. GCase and GAPDH are positive and negative controls, respectively. Right, quantification of normalized CANX levels from the Con-A pulldown. **F)** Analysis of GCase solubility was done as in panel A in day 90 *SNCA*-3X DA neurons treated with scrambled (scrb) or RyR3 shRNA knock-down (KD) lentivirus (MOI=5, dpi 2 weeks), For all quantifications, values are mean ± SEM, $*p < 0.05$; $***p < 0.001$; $****p < 0.0001$; ns = not significant, using student's unpaired t-test.

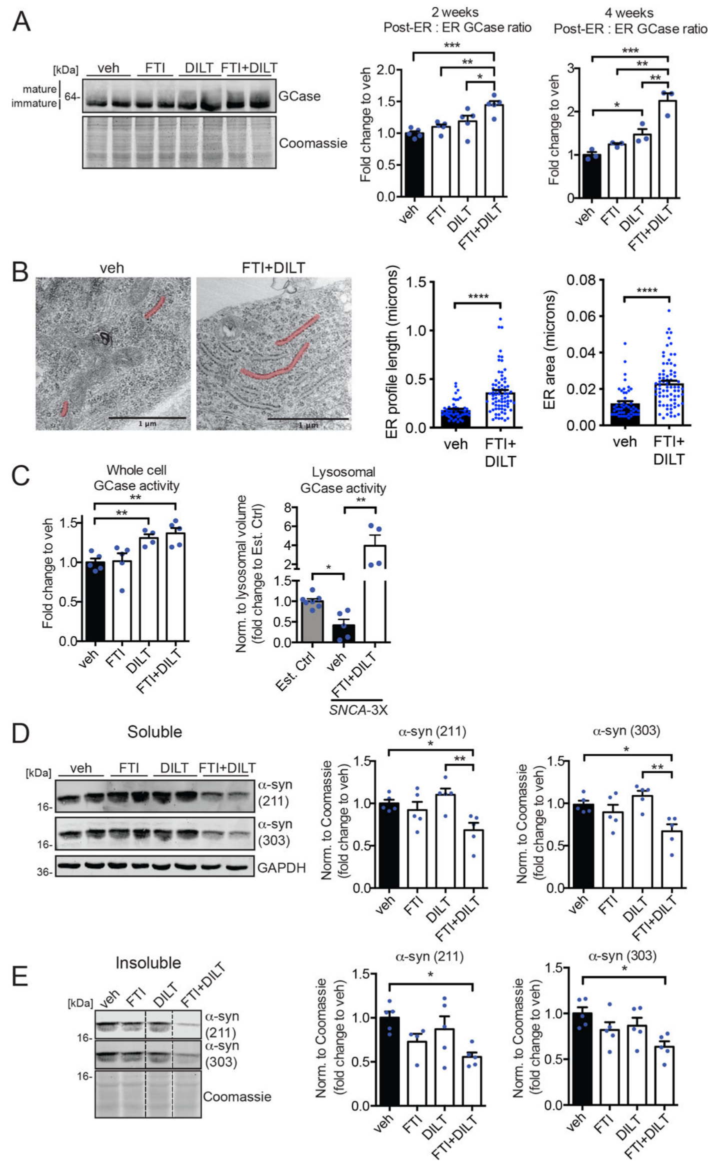

Figure 7. Rescue of ER fragmentation and lysosomal GCase by synergistic enhancement of ER proteostasis and trafficking.

SNCA-3X DA neurons were treated with vehicle, 5nM farnesyl transferase inhibitor (FTI), 25uM diltiazem (DILT), or combined FTI+DILT. **(A)** GCase western blot of day 90 3x-1 DA neurons treated with FTI+DILT for 2 weeks. Coomassie is shown as a loading control. Quantification of combined data from 3X-1, 2, is shown to the right. **B)** Electron microscopy analysis of day 90 *SNCA*-3X DA neurons (shown, 3X-2) treated with DMSO vehicle or FTI+DILT for 2 weeks. Quantification of ER morphology is shown on the right (segments highlighted in red). Scale bar, 1μm. **C)** Left, whole cell GCase activity of treated 3x-1 and 3x-2 lysates from panel A. Right, analysis of live cell lysosomal GCase activity of FTI+DILT treated 3x-2 DA neurons and compared to healthy controls (Est. Ctrl). **D)** Western blot of soluble a-syn. The same membranes from panel A were sequentially probed with syn211 then syn303 anti-α-syn antibodies. GAPDH is shown as a loading control. Right, α-syn quantification. **E)** Western blot of insoluble a-syn in day 90 *SNCA*-3X

DA neurons treated with FTI+DILT for 2 weeks. The same membranes were sequentially probed with syn211 then syn303. Irrelevant lanes were cropped, indicated by a dashed line. Quantification is shown to the right. For all quantifications, values are mean ± SEM, *p < 0.05; **p < 0.01; ***p < 0.001; ****p < 0.0001, using student's unpaired t-test (panels B, C right) or ANOVA with Tukey's post-hoc test (panels A, D, C (left), E).

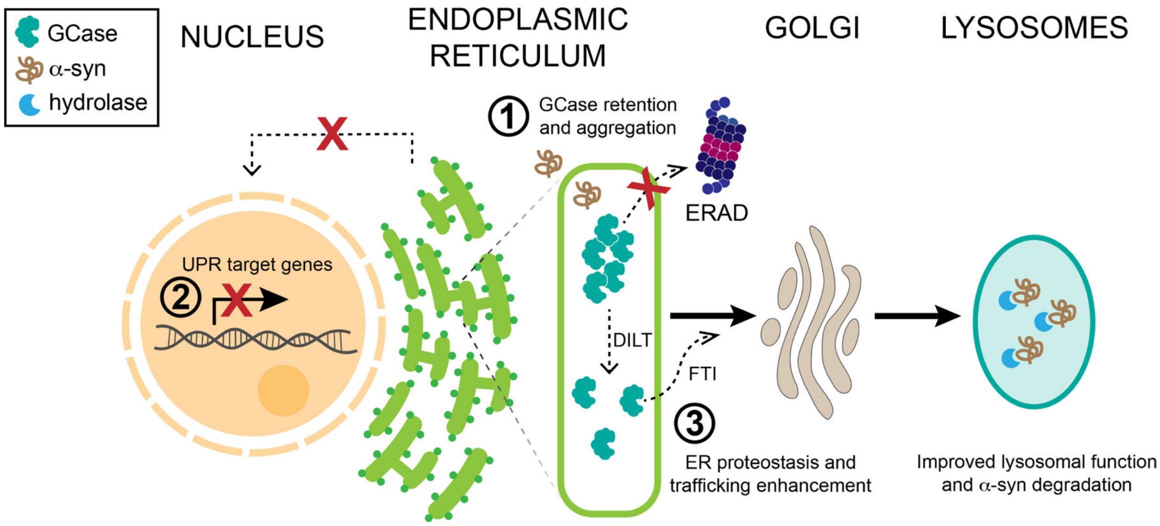

Figure 8. Proteostasis dysfunction and rescue in PD patient neurons.

Accumulation of α-synuclein (α-syn) at the ER is associated with ER fragmentation, accumulation and aggregation of immature β−glucocerebrosidase (GCase), and failure of UPR activation (1, 2). Enhancing ER folding capacity promotes the formation of soluble, active GCase, while combined treatment with protein trafficking enhancers rescues lysosomal function and reduces pathological α-syn (3).

KEY RESOURCES TABLE

REAGENT or RESOURCE	SOURCE	IDENTIFIER
Antibodies		
Rabbit polyclonal anti-alpha synuclein (C-20)	Santa Cruz	Cat #sc-7011-R RRID: AB_2192953
Mouse monoclonal anti-alpha synuclein (LB509)	Abcam	Cat #ab27766 RRID: AB_727020
Mouse monoclonal anti-alpha synuclein (syn211)	Sigma Aldrich	Cat #S5566 RRID: AB_261518
Mouse monoclonal anti-alpha synuclein (303)	Biolegend	Cat #824301 RRID: AB_2564879
Mouse monoclonal anti-β3-tubulin	Biolegend	Cat #802001 RRID: AB_2564645
Rabbit polyclonal anti-calnexin (CANX)	Cell Signaling	Cat #2433S RRID: AB_2243887
Mouse monoclonal anti-calnexin (CANX) (E-10)	Santa Cruz	Cat #sc-46669 RRID: AB_626784
Mouse monoclonal anti-cathepsin D	Sigma	Cat #C0715 RRID: AB_258707
Mouse monoclonal anti-EDEM1	Santa Cruz	Cat #sc-377394
Rabbit polyclonal anti-p-eIF2α (ser51)	Cell Signaling	Cat #3398 RRID: AB_2096481
Mouse monoclonal anti-eIF2α	Santa Cruz	Cat #sc-133132 RRID: AB_1562699
Mouse monoclonal anti-FoxA2	Santa Cruz	Cat #sc-101060 RRID: AB_1124660
Mouse monoclonal anti-GAPDH	Millipore	Cat #CB1001 RRID: AB_2107426
Rabbit polyclonal anti-glucocerebrosidase (GCase)	Sigma	Cat #G4171 RRID: AB_1078958
Mouse monoclonal anti-glucocerebrosidase (GCase) (8E4)	N/A (gift from J. Aerts) Barneveld et al, Eur. J. Biochem. 134, 585–589 (1983)	N/A
Rabbit polyclonal anti-GRP78	Novus	Cat #NBP1-06274 RRID: AB_1555284
Mouse monoclonal anti-GRP94	Santa Cruz	Cat #sc-393402
Mouse monoclonal anti-Hexosaminidase B (HexB)	Sigma	Cat #sc-376781
Rabbit polyclonal anti-Nanog	Abcam	Cat #ab21624 RRID: AB_446437
Neurofilament	Biolegend	Cat #SMI-312R RRID: AB_2314906
Rabbit polyclonal anti-Oct4	Abcam	Cat #ab19857 RRID: AB_445175
Rabbit polyclonal anti-PDI	Abcam	Cat #ab11432 RRID: AB_298038
Rabbit polyclonal anti-Sox2	Abcam	Cat #ab97959 RRID: AB_2341193
Mouse monoclonal anti-SSEA4	Abcam	Cat #ab16287 RRID: AB_778073

REAGENT or RESOURCE	SOURCE	IDENTIFIER
Mouse monoclonal anti-Tra-1-60	Abcam	Cat #ab16288 RRID: AB_778563
Rabbit polyclonal anti-tyrosine hydroxylase (TH)	Millipore	Cat #AB5986 RRID: AB_92190
Rabbit polyclonal anti-ubiquitin	Dako	Cat #Z045801-5
Mouse monoclonal anti-ykt6	Santa Cruz	Cat #SC-365732 RRID: AB_10859388
Secondary antibody: Alexa Fluor 488 Goat anti-rabbit IgG secondary (H+L)	Invitrogen	Cat #A11034 RRID: AB_2576217
Secondary antibody: Alexa Fluor 488 Goat anti-mouse IgG secondary (H+L)	Invitrogen	Cat #A11029 RRID: AB_138404
Secondary antibody: Alexa Fluor 568 Goat anti-rabbit IgG secondary (H+L)	Invitrogen	Cat #A11036 RRID: AB_10563566
Secondary antibody: Alexa Fluor 568 Goat anti-mouse IgG secondary (H+L)	Invitrogen	Cat #A11031 RRID: AB_144696
Secondary antibody: Alexa Fluor 680 Goat anti-mouse IgG secondary (H+L)	Invitrogen	Cat #A21058 RRID: AB_2535724
Secondary antibody: IRdye 800CW goat anti-mouse IgG secondary (H+L)	Li-Cor Biosciences	Cat #926-32210 RRID: AB_621842
Secondary antibody: IRdye 800CW goat anti-rabbit IgG secondary (H+L)	Li-Cor Biosciences	Cat #926-32211 RRID: AB_621843
Bacterial and virus strains		
pER4 (vector) lentivirus	Mazzulli et al., 2011	N/A
pER4 ykt6-CS lentivirus	Cuddy et al., 2019	N/A
Scrambled (scrb) shRNA lentivirus	This paper	N/A
RyR3 shRNA lentivirus	This paper	N/A
pER4 GBA1 L444P lentivirus	This paper	N/A
Biological samples		
Human brain tissue of control, DLB, DLB + AD patients	Northwestern University Alzheimer's disease pathology core (CNADC). Please refer to Table 1 for more details	N/A
Mouse Brain tissue from LIMP2-/- mice	Rothaug et al., 2014	N/A
Chemicals, peptides, and recombinant proteins		
Bafilomycin A1	Santa Cruz	Cat #SC-201550
Bovine serum albumin (BSA), heat shock, fatty acid free	Roche	Cat #03117057001
Brefeldin A (BFA)	Cell Signaling	Cat #9972S
Cascade Dextran Blue	Life Technologies	Cat #D1976
CHAPS hydrate	Sigma	Cat #C5070
Conduritol β epoxide (CBE)	Millipore	Cat #234599
Doxycycline (DOX)	Sigma	Cat #D3447
Diltiazem hydrochloride (DILT)	Sigma	Cat #D2521
Dantrolene sodium salt (DANT)	Sigma	Cat #D9175
DHBP (1,1'-diheptyl-4,4'-bipyridinium dibromide)	Sigma	Cat #180858
Epoxomicin	Fisher	Cat #10007806
Farnesyl transferase inhibitor (FTI): LNK-754	Link Medicine	N/A

REAGENT or RESOURCE	SOURCE	IDENTIFIER
Fetal bovine serum (FBS), heat-inactivated	Thermo Fisher Scientific	Cat #10438026
Geneticin (G418)	Thermo Fisher Scientific	Cat #10131027
L-glutamine	Gibco	Cat #25030081
Glutaraldehyde, 25% aqueous solution	Electron Microscopy Sciences	Cat #16220
Hygromycin B	Thermo Fisher Scientific	Cat #10687010
LX112	Ladd Research Industries	Cat #21310
Normal goat serum (NGS)	Jackson ImmunoResearch	Cat #005-000-121
Osmium tetroxide (OsO_4), 4% aqueous solution	Electron Microscopy Sciences	Cat #19150
Paraformaldehyde (10%, methanol-free)	Polysciences, Inc.	Cat #40181
Penicillin / Streptomycin	Thermo Fisher Scientific	Cat #10378016
Phenylmethylsulfonyl fluoride (PMSF)	Sigma	Cat #78830
Protease Inhibitor Cocktail (PIC)	Roche	Cat #11836170001
N-Lauroylsarcosine sodium salt (sarkosyl)	Sigma	Cat #L9150
Sodium dodecyl sulfate (SDS)	Sigma	Cat #L4509
Sodium orthovanadate (Na_3VO_4)	Sigma	Cat #450243
Sodium fluoride (NaF)	Sigma	Cat #201154
Sucrose	Sigma	Cat #S1888
Triton X-100	Sigma	Cat #T8787
Thapsigargin (Tg)	Sigma	Cat #T9033
Thioflavin S (ThioS)	Sigma	Cat #T1892
Uranyl acetate	Electron Microscopy Sciences	Cat #22400
Methyl-5-Norbornene-2,3-Dicarboxylic Anhydride (NMA)	Electron Microscopy Sciences	Cat #19000
Dodecenyl Succinic Anhydride (DDSA)	Electron Microscopy Sciences	Cat #13700
2,4,6-Tri(dimethylaminomethyl) phenol (DMP-30)	Electron Microscopy Sciences	Cat #13600
5-(pentafluoro-benzoylamino) fluorescein di-ß-D-glucopyranoside (PFB-FDGluc)	Life Technologies	Cat #P11947
4-methylumbelliferyl β-glucopyranoside (4-MU-Gluc)	Chem-Impex Int’l Inc.	Cat #21630
Critical commercial assays		
CellTag 700	Li-Cor Biosciences	Cat #926-41090
Concanavalin A (CON-A), biotinylated	Vector Laboratories	Cat #B-1005-5
DNeasy Blood and Tissue Kit	QIAGEN	Cat #69504
Duolink In Situ Red Starter Kit Mouse/Rabbit	Sigma Aldrich	Cat #92101
Endoglycosidase H	New England Biolabs	Cat #P0702L
HIV1-p24 Antigen ELISA Kit	Zeptometrix	Cat #0801111
Pierce BCA Protein Assay Kit	Thermo Fisher Scientific	Cat #23227
PureLink Genomic DNA Kit	Invitrogen	Cat #K182002
RevertAid First Strand cDNA Synthesis Kit	Thermo Fisher Scientific	Cat #K1621
RNeasy Mini Prep Kit	QIAGEN	Cat #74104
T7EI Endonuclease I assay kit	Genecopoeia	Cat #IC005
Quantitative RT-PCR: SNCA (ID: Hs00240906_m1)	Thermo Fisher Scientific	Cat #4331182

REAGENT or RESOURCE	SOURCE	IDENTIFIER
Quantitative RT-PCR: GRP78 (ID: Hs99999174_m1)	Thermo Fisher Scientific	Cat #4331182
Quantitative RT-PCR: CANX (ID: Hs01558409_m1)	Thermo Fisher Scientific	Cat #4331182
Quantitative RT-PCR: EDEM1 (ID: Hs00976004_m1)	Thermo Fisher Scientific	Cat #4331182
Quantitative RT-PCR: XBP1-S (ID: Hs03929085_g1)	Thermo Fisher Scientific	Cat #4331182
Quantitative RT-PCR: RyR3 (ID: Hs00168821_m1)	Thermo Fisher Scientific	Cat #4331182
Quantitative RT-PCR: GBA1 (ID: Hs00164683_m1)	Thermo Fisher Scientific	Cat #4331182
Quantitative RT-PCR: Nanog (ID: Hs04399610_g1)	Thermo Fisher Scientific	Cat #4331182
Quantitative RT-PCR: Puromycin (Custom Assay# gi763524_CCN1FIY)	Thermo Fisher Scientific	Cat #4331182
Quantitative RT-PCR: RNAseP (ID: 4403326)	Thermo Fisher Scientific	Cat #4331182
Quantitative RT-PCR: ACTB (β-actin) (ID: Hs99999903_m1)	Thermo Fisher Scientific	Cat #4331182
Quantitative RT-PCR: GAPDH (ID: Hs02758991_g1)	Thermo Fisher Scientific	Cat #4331182
QuikChange XL Site-Directed Mutagenesis Kit	Agilent	Cat #200517
Deposited data		
Experimental models: Cell lines		
H4 neuroglioma cells	Mazzulli et al., 2011; From: Pamela McLean (Mayo Clinic, Jacksonville, Florida, USA)	N/A
GM15010 (*SNCA* Triplication, 3x-1)	This paper; clinical and other information can be obtained from the Coriell Cell Repository	N/A
ND00196 (*SNCA* Triplication, 3x-2)	This paper; clinical and other information can be obtained from the Coriell Cell Repository	N/A
ND00139 (*SNCA* Triplication, 3x-4)	This paper; clinical and other information can be obtained from the Coriell Cell Repository	N/A
ND34391 (*SNCA* Triplication, Est. 3X).	Mazzulli et al., 2016a; Zunke et al., 2018; Cuddy et al., 2019; Coriell Cell Repository	N/A
GM00852, GD patient (N370S / 84GG)	Mazzulli et al., 2011; Mazzulli et al., 2016a; Coriell Cell Repository	N/A
ND34982, GBA1-PD heterozygote (N370S / WT)	Coriell Cell Repository	N/A
GD patient L444P / L444P	Schondorf et al., Nat. Comm. 2014	N/A
A53T alpha-synuclein and isogenic control	Soldner et al., Cell, 2011	N/A
Experimental models: Organisms/strains		
Oligonucleotides- See Table S4		
Recombinant DNA		
pCXLE-hOCT3/4-shp53-F	Addgene, Okita et al Nat Methods. 2011	Cat #27077
pCXLE-hUL	Addgene, Okita et al Nat Methods. 2011	Cat #27080
pCXLE-hSK	Addgene, Okita et al Nat Methods. 2011	Cat #27078
PITX3-2A-eGFP-PGK-Puro	Addgene, Hockemeyer et al Nat Biotechnol. 2011	Cat #31943
Cas9-nickase plasmid PX335	Addgene, Nora et al Cell. 2017	Cat #42335

REAGENT or RESOURCE	SOURCE	IDENTIFIER
pLKO.1 RyR3 shRNA (clone ID #TRCN0000053349)	Sigma	Cat #NM_001036
pER4-ykt6-CS	This paper	N/A
pER4-GBA1 L444P	This paper	N/A
Software and algorithms		
GraphPad Prism V6.0 software	GraphPad	https://www.graphpad.com/scientific-software/prism/
ImageJ / Fiji V1.0 software	National Institutes of Health	https://imagej.net/software/fiji/
Nikon NIS Elements	Nikon	https://www.microscope.healthcare.nikon.com/products/software/nis-elements
Odyssey software (Image Studio V3.1.4)	Li-Cor Biosciences	https://www.licor.com/bio/image-studio/
Snapgene V5.3 software	SnapGene	https://www.snapgene.com
Other		
Concanavalin-A, biotinylated	Vector Laboratories	Cat #B-1005-5
DAPI Fluoromount mounting media	Southern Biotech	Cat #0100-20
Intercept blocking buffer	Li-Cor Biosciences	Cat #927-70001
Lenti-X concentrator	Clontech	Cat #631232
Lipofectamine 3000	Thermo Fisher Scientific	Cat #L3000008
Matrigel	Fisher	Cat #CB-40234
mTeSR1 media	StemCell Technologies	Cat #85850
Neurobasal SM1 media	Thermo Fisher Scientific	Cat #21103-049
NeuroCult SM1 supplement	StemCell Technologies	Cat #05711
NeutrAvidin agarose beads	Thermo Fisher Scientific	Cat #29204
PVDF transfer membrane, 0.45 mm pore size	Millipore	Cat #IPFL00010
X-tremeGENE HP DNA Transfection Reagent	Roche	Cat #6366236001